Acta Geotechnica (2019) 14:1379–1401
https://doi.org/10.1007/s11440-018-0735-5

RESEARCH PAPER

Influence of initial state and intermediate principal stress on undrained behavior of soft clay during pure principal stress rotation

Yuke Wang[1,2,3] · Yufeng Gao[2,4] · Bing Li[5] · Lin Guo[6] · Yuanqiang Cai[7] · Ali H. Mahfouz[8]

Received: 20 December 2017 / Accepted: 9 October 2018 / Published online: 17 October 2018

Abstract

It is important to be fully aware of the dynamic characteristics of saturated soft clays under complex loading conditions in practice. In this paper, a series of undrained tests for soft clay consolidated with different initial major principal stress direction ξ were conducted by a hollow cylinder apparatus (HCA). The clay samples were subjected to pure principal stress rotation as the magnitudes of the mean total stress p, intermediate principal stress coefficient b, and deviator stress q were all maintained constant. The influences of intermediate principal stress coefficient and initial major principal stress direction on the variation of strain components, generation of pore water pressure, cyclic degradation and non-coaxiality were investigated. The experimental observations indicated that the strain components of specimen were affected by both intermediate principal stress coefficient and initial major principal stress direction. The generation of the pore water pressure was significantly influenced by intermediate principal stress coefficient. However, the generation of pore water pressure was merely influenced by initial major principal stress direction when $b = 0.5$. It was also noted that the torsional stress–strain relationships were affected by the number of cycles, and the effect of intermediate principal stress coefficient and initial major principal stress direction on the torsional stress–strain loops were also significant. Stiffness degradation occur under pure principal stress rotation. Anisotropic behavior resulting from the process of inclined consolidation have considerable effects on the strain components and non-coaxial behavior of soft clay.

Keywords Initial major principal stress direction · Intermediate principal stress coefficient · Natural soft clay · Non-coaxiality · Pore water pressure · Pure principal stress rotation · Strain components

✉ Yufeng Gao
yfgao66@163.com

Yuke Wang
ykewang@163.com

[1] College of Water Conservancy and Environmental Engineering, Zhengzhou University, No. 100, Science Road, Zhengzhou 450001, People's Republic of China

[2] Key Laboratory of Ministry of Education for Geomechanics and Embankment Engineering, Hohai University, No. 1, Xikang Road, Nanjing 210098, People's Republic of China

[3] Collaborative Innovation Center of Water Conservancy and Transportation Infrastructure Safety Protection, Henan Province, Zhengzhou University, Zhengzhou, Henan 450001, People's Republic of China

[4] Jiangsu Research Center for Geotechnical Engineering Technology, Hohai University, No. 1, Xikang Road, Nanjing 210098, People's Republic of China

[5] College of Civil Engineering, Southeast University, Nanjing 210096, People's Republic of China

[6] College of Architecture and Civil Engineering, Wenzhou University, Wenzhou 325035, People's Republic of China

[7] Key Laboratory of Soft Soils and Geoenvironmental Engineering, Ministry of Education, Zhejiang University, Hangzhou 310027, People's Republic of China

[8] Faculty of Petroleum and Mining Engineering, Suez University, Suez 43721, Egypt

1 Introduction

The geotechnical problem of soft clay is widespread in Wenzhou, a coastal city in China. Being one of the most developed areas in China, a large number of infrastructures have been constructed on this kind of soil. The soil grounds of these projects may undergo long-term cyclic loads during construction and operation period. The disturbance of soil layer and the reduction of bearing capacity, due to the effect of cyclic loads like waves, may result in foundation instability, huge loss of life and property. The displacement and rearrangement of soil particles will be caused by cyclic load as wave load, the major principal stress direction is rotated away from the vertical by an angle during consolidation, which leads to anisotropic 'inclined' consolidation. The anisotropy in stress–strain relationship, strength and other mechanical behavior occurs due to the different consolidation states. Meanwhile, seabed and marine structure foundation are subjected to complex stresses under wave loads, which induces dynamic stress, dynamic strain and generation of pore water pressure [23]. For example, in Bohai region of China, the cyclic wave load caused platform sliding and inclining, and the deposition distance of one petroleum pipeline in Bohai gulf went over certain limits. The second west breakwater of Niigata port destroyed under storm activity. They are all closely related to complex loads involved principal stress rotation. Therefore, it is important to be fully aware of the dynamic characteristics of saturated soft clays under complex loading condition.

As described in detail by Wang et al. [21], wave load, a special kind of cyclic load with reciprocation for a long time, is different from the static load and the seismic load. According to Ishihara and Towhata [3], the cyclic variation of vertical stress is 90 degrees out of phase with the cyclic change in the horizontal shear stress. During the cyclic alteration of these two components of shear stress, the soil element is subjected to continuous rotation of the principal stress direction.

In recent years, many investigations focused on cases under complex loading conditions involving principal stress direction rotation during shearing. Ishihara and Towhata [3] examined the impact of the principal stress axes rotating on undrained behavior of saturated sand by cyclic triaxial–torsional shear tests. Miura et al. [8] carried out a series of drained tests under more general stress condition involving principal stress rotation. In their tests, it was found that the effect of rotation of principal stress axis cannot be negligible. However, as pointed out by Shibuya et al. [16], due to the limitation of their apparatus, the principal stress rotation was not independent of intermediate principal stress coefficient. Based on the limitation mentioned above, a new hollow cylinder apparatus was developed by Hight et al. [2]. Then, different conditions including initial anisotropy, different intermediate principal stress coefficient and principal stress rotation can be investigated. Symes et al. [17] investigated the effect of principal stress rotation on undrained anisotropy of sand at a constant stress during both monotonic and cyclic loading, drained tests were also conducted [18]. Nakata et al. [9] found that pore pressures and strains were accumulated under the principal stresses rotation although the deviator stress remains constant. However, the intermediate principal stress coefficient in these tests were all fixed to 0.5. Yang et al. [28] were among the first to study the effect of different intermediate principal stress coefficients on the undrained behavior of soils and found it had significant impact. Based on the research, Tong et al. [19] conducted a series of tests to study the effect of intermediate principal stress coefficient on drained behavior of sands under principal stress rotation. Similar conclusions are obtained that the effect of different intermediate principal stress coefficients on the response of sand is significant.

The soft clay under complex loading involved principal stress rotation has been investigated by many researchers. Wang et al. [24] investigated the anisotropic deformation behavior and shear strength of Wenzhou natural soft marine clay by HCA, the influence of intermediate principal stress and principal stress direction on deformation behavior of soft clay were discussed in detail. Shen et al. [15] conducted comprehensive tests including cyclic principal stress rotation, cyclic shear with abrupt change of principal stress orientation and cyclic shear, with fixed principal stress orientation to obtain the critical behavior of Hangzhou intact soft clay. In order to investigate cyclic deformation behavior of natural soft marine clay, Wang et al. [22] conducted a series of undrained tests with the deviator stress kept at a constant level as principal stress rotating 5000 cycles. Zhou and Xu [30] also found that the influence of shear stress level on strain development was remarkable by different types of tests, including a shearing test along fixed principal stress direction, a pure rotation test, and both clockwise and anti-clockwise rotation tests. A series of cyclic heart-shaped and cyclic triaxial undrained tests were performed on Shanghai clay through simultaneously varying the torsional shear stress and the normal stresses, the plastic shakedown behavior of saturated clay subjected to traffic loading with principal stress rotation was discussed in detail by Qian et al. [12, 13].

However, the reports summarized above are all conducted by fixing the major principal stress axis in the vertical direction prior to shear in the experiments. In actual field conditions, the direction of major principal stress is not always parallel to the vertical during process of consolidation. Many field loading situations, such as wave

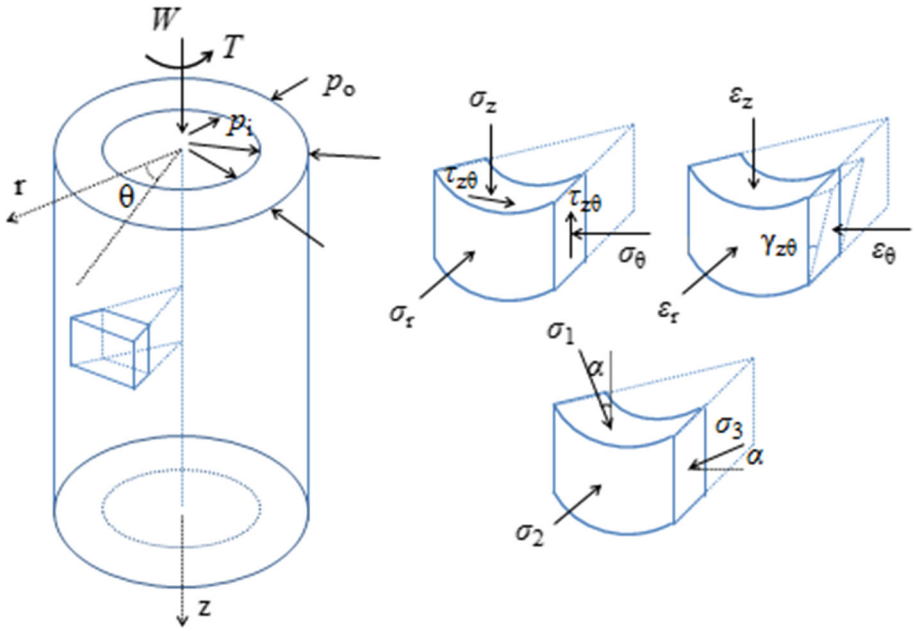

Fig. 1 Stress and strain states in hollow cylinder specimen

loading on seabed deposits, seismic excitation in level ground, and traffic loadings on the sub-grade, may involve significant rotation of the principal stress directions. However, little is known concerning the effects of anisotropic 'inclined' consolidated. Multi-stage embankments built on soft marine ground, which rely on foundation strength improvements taking place by consolidation under load, provide the best-known practical example of this condition. Jardine and Smith [4] focused on the effects of anisotropic 'inclined' consolidation, where the major principal stress direction is rotated away from the vertical by an angle during consolidation, and presented a numerical simulation of a multi-stage embankment, including detailed predictions of stress conditions developed in the foundation designed by a 'consolidated undrained' approach. Zdravkovic and Jardine [29] conducted experimental investigations on dense silt samples involving principal stress rotation during consolidation, they pointed out that although the effective stress paths were guided by the conditions of multi-stage embankments built on soft ground, the results have considerable significance in other practical geotechnical problems. Considering that little attention was given to the effect of anisotropic consolidation on the deformation behavior of soil involved various loading conditions, Xiong et al. [26] studied the impacts of anisotropy on deformation behavior by using a hollow cylinder apparatus, the tests that sheared with a fixed principal stress direction and tests that sheared with a constant deviator stress under pure principal stress rotation alone are both studied. With the rapid development of coastal cities, numerous buildings and infrastructures have been built on soft clay foundations. The geotechnical problems existing in soft clay have drawn attention to many researchers. To the authors' concern, there have been little studies of tests on the behavior of soft clay involved anisotropic 'inclined' consolidations reported in the literature.

Based on the consideration above, in this study, a series of undrained HCA tests involving pure principal stress rotation on soft clay with different initial major principal stress directions were carried out, the effect of intermediate principal stress coefficient was also studied. The emphasis of this paper was placed on the impact of intermediate principal stress and initial state on strain components development, pore water pressure and non-coaxiality of the anisotropic 'inclined' consolidation soft clay.

2 Sampling preparation and test procedures

In this paper, the natural soft clay used was obtained from a pit of a depth of 3–6 m below the ground surface from the coastal zone in Wenzhou, a coastal city in eastern China. All clay samples were obtained by pressing thin-walled tubes slowly into a horizontal bench prepared in the pit, the diameter of the tubes is 150 mm and the length of the tubes is 250 mm. After that, the tubes were excavated from the pit and then sealed at the both ends. They would be transported to the laboratory and stored in a humidity room until they were used for testing. The details of the sampling procedure were explained by Kirkgard and Lade [5]. The primary physical index properties of this Wenzhou clay are

Table 1 Equations used for calculation of stress of stress and strain components

	Stress	Strain
Vertical	$\sigma_z = \frac{W}{\left(r_0^2 - r_i^2\right)} + \frac{p_0 r_0^2 - p_i r_i^2}{\left(r_0^2 - r_i^2\right)}$	$\varepsilon_z = -\frac{z}{H}$
Circumferential	$\sigma_\theta = \frac{p_0 r_0 - p_i r_i}{(r_0 - r_i)}$	$\varepsilon_\theta = -\frac{u_0 + u_i}{(r_0 + r_i)}$
Radial	$\sigma_r = \frac{p_0 r_0 + p_i r_i}{(r_0 + r_i)}$	$\varepsilon_r = -\frac{u_0 - u_i}{(r_0 - r_i)}$
Torsional shear	$\tau_{z\theta} = \frac{3M_T}{2\left(r_0^3 - r_i^3\right)}$	$\gamma_{z\theta} = -\frac{2\theta\left(r_0^3 - r_i^3\right)}{3H\left(r_0^2 - r_i^2\right)}$
Major principal	$\sigma_1 = \frac{\sigma_z + \sigma_\theta}{2} + \sqrt{\left(\frac{\sigma_z - \sigma_\theta}{2}\right)^2 + \tau_{z\theta}^2}$	$\varepsilon_1 = \frac{\varepsilon_z + \varepsilon_\theta}{2} + \sqrt{\left(\frac{\varepsilon_z - \varepsilon_\theta}{2}\right)^2 + \gamma_{z\theta}^2}$
Intermediate principal	$\sigma_2 = \sigma_r$	$\varepsilon_2 = \varepsilon_r$
Minor principal	$\sigma_3 = \frac{\sigma_z + \sigma_\theta}{2} - \sqrt{\left(\frac{\sigma_z - \sigma_\theta}{2}\right)^2 + \tau_{z\theta}^2}$	$\varepsilon_3 = \frac{\varepsilon_z + \varepsilon_\theta}{2} - \sqrt{\left(\frac{\varepsilon_z - \varepsilon_\theta}{2}\right)^2 + \gamma_{z\theta}^2}$

specific gravity, G_s = 2.70; water content, w_n = 59–62%; initial density, ρ_o = 1.61–1.65 g/cm^3; initial void ratio, e_0 = 1.64–1.71; plasticity gravity, w_p = 33; liquid limit, w_L = 65; clay fraction, 41%, silt friction is 55% and plasticity index, I_p = 36.

The hollow cylinder apparatus has four subsystems responsible for the control of the axial load W, torque M_T, and internal and external pressures p_i and p_o, respectively, such that complex stress path involving the change of the principal stress direction can be achieved. In the hollow cylinder apparatus, the outer diameter r_o, inner diameter r_i and height H of test clay specimens were 100 mm, 60 mm, and 200 mm, respectively. The clay specimens were trimmed by a specialized tool and then placed on the base pedestal and enclosed with the inner and outer membrane. Then, the specimens were first saturated at a back pressure of 200 kPa with an effective stress of 10 kPa. The b-value check was conducted to guarantee that b-value greater than 0.98 for all tests. After that, the specimens in the tests were anisotropic consolidated to the same stress state with p' = 100 kPa. In order to investigate the effects of anisotropy due to different initial state on the deformation behavior of soft clay, the process of anisotropic consolidation conducted by Zdravkovic and Jardine [29] was adopted, different b-values and different initial major principal stress directions ζ with respect to vertical axis are considered.

The description of the control system used in this paper was introduced in detail by Wang et al. [20]. The pressures applied to a hollow cylindrical specimen are illustrated in Fig. 1. The equations used for stress and strain components in HCA tests, which are based mainly on the studies of Hight et al. [2], are listed in Table 1.

After the anisotropic consolidation with different initial major principal stress directions ξ, the specimens were then sheared under pure principal stress rotation, with constant deviator stress during the rotation of the principal stress axis. The rate of principal stress rotation was 0.4°/min. Different intermediate principal stress coefficient b = 0, 0.5, 1 and different initial major principal stress directions ζ = 0°, 30°, 45°, 60°, 90° were considered. The test schemes are listed in Table 2.

Table 2 Parameters adopted in hollow cylinder tests

Test ID	ζ (°)	p' (kPa)	b	q (kPa)	□(°)/N □
R1					
R100	0°	100	0	40	0-900/5
R105			0.5		
R110			1		
R2					
R200	30°		0		
R205			0.5		
R210			1		
R3					
R300	45°		0		
R305			0.5		
R310			1		
R4					
R400	60°		0		
R405			0.5		
R410			1		
R5					
R500	90°		0		
R505			0.5		
R510			1		

The equations of major principal stress direction α, the intermediate principal stress coefficient b, deviator stress q, and mean principal stress p are as following:

$$\alpha = \frac{1}{2}\arctan\frac{2\tau}{\sigma_z - \sigma_\theta} \quad (1)$$

$$b = (\sigma_2 - \sigma_3)/(\sigma_1 - \sigma_3) \quad (2)$$

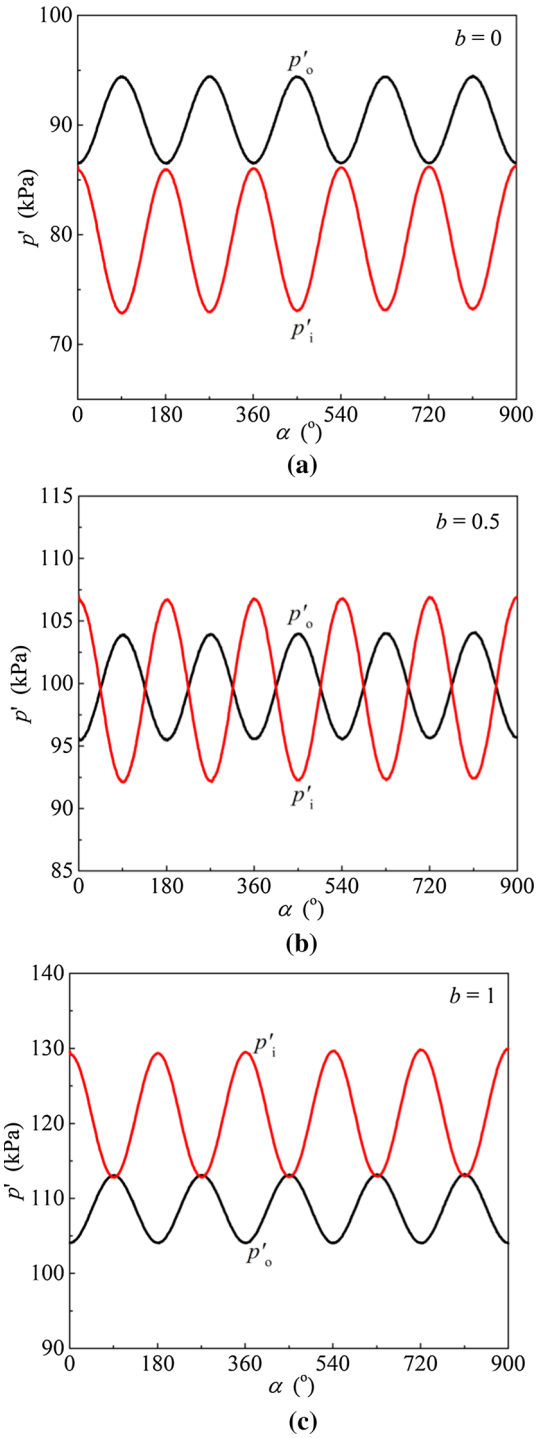

Fig. 2 Variation of outer and inner cell pressures under rotational shear: **a** $b = 0$; **b** $b = 0.5$; **c** $b = 1$

$$q = \sqrt{\frac{(\sigma_1 - \sigma_2)^2 + (\sigma_2 - \sigma_3)^2 + (\sigma_1 - \sigma_3)^2}{2}} \quad (3)$$

$$p = (\sigma_1 + \sigma_2 + \sigma_3)/3 \quad (4)$$

Figure 2 presents the variation of outer and inner cell pressures under pure principal stress rotation for $b = 0$, 0.5, 1 under $\zeta = 0°$. The variations of vertical load and torque are shown in Fig. 3 for $b = 0$, 0.5, 1 under $\zeta = 0°$. It can be observed that, with the similar pattern of variation of the vertical load and torque, the variation of the outer and inner cell pressures showed different patterns in terms of the amplitude and phase for different b-values. Figure 4 shows the deviator stress path in the $\tau_{z\theta} - (\sigma_z - \sigma_\theta)/2$ plane, where σ_z is the vertical normal stress and σ_θ is the horizontal normal stress.

3 Test results and discussion

Undisturbed soft clay is inherently anisotropic resulting from orientation in the deposition process. Deformation is caused by both variations in the magnitudes of the principal stresses and the changes in the orientation with reference to the depositional plane. As reported by Wang et al. [20, 24], the strain components of the soft clay under monotonic tests are affected by both intermediate principal stress coefficient b and major principal stress directions α. The shear strength of Wenzhou soft clay from monotonic tests are different for different α angles under the same strain level, while the difference gradually reduces when the strain level is high. As shown in Fig. 5, the strength of soft clay is dependent on different b-values and α angles, similar to undisturbed San Francisco clay by Lade and Kirkgrad [7], London clay [10], Hangzhou clay [31] and Shanghai clay [14], which should be considered in the geotechnical engineering design with great caution.

Figure 6 shows the typical evolution of four normal strain components (take contraction as positive) with increase in principal stress direction for test series R1 under $b = 0$, 0.5, 1. It can be seen that the development styles of strain components differ and depend on b-value, it is similar to the undrained results of intact natural Hangzhou soft clay [31] and Shanghai soft clay [14] under pure principal stress rotation. To further investigate the influence of coefficient b on the deformation characteristics of specimens, the evolutions of the strain components ε_z, $\gamma_{z\theta}$, ε_θ, ε_r for varying $b = 0$, 0.5, 1 with varying initial major principal stress directions ζ are shown in Figs. 7, 8, 9, 10, respectively.

Figure 7 shows the effect of coefficient b on the evolutions of axial strain ε_z for different test series. Take Fig. 7a as an example, in a rotation period (0°–180°), ε_z increases in tensile side and then decreases gradually. With the increasing rotation cycles, the accumulation of ε_z occur. At the end of each cycle ($\alpha = 180°$, 360°, 540°, 720°, 900°), the specimens are subjected to compression in the

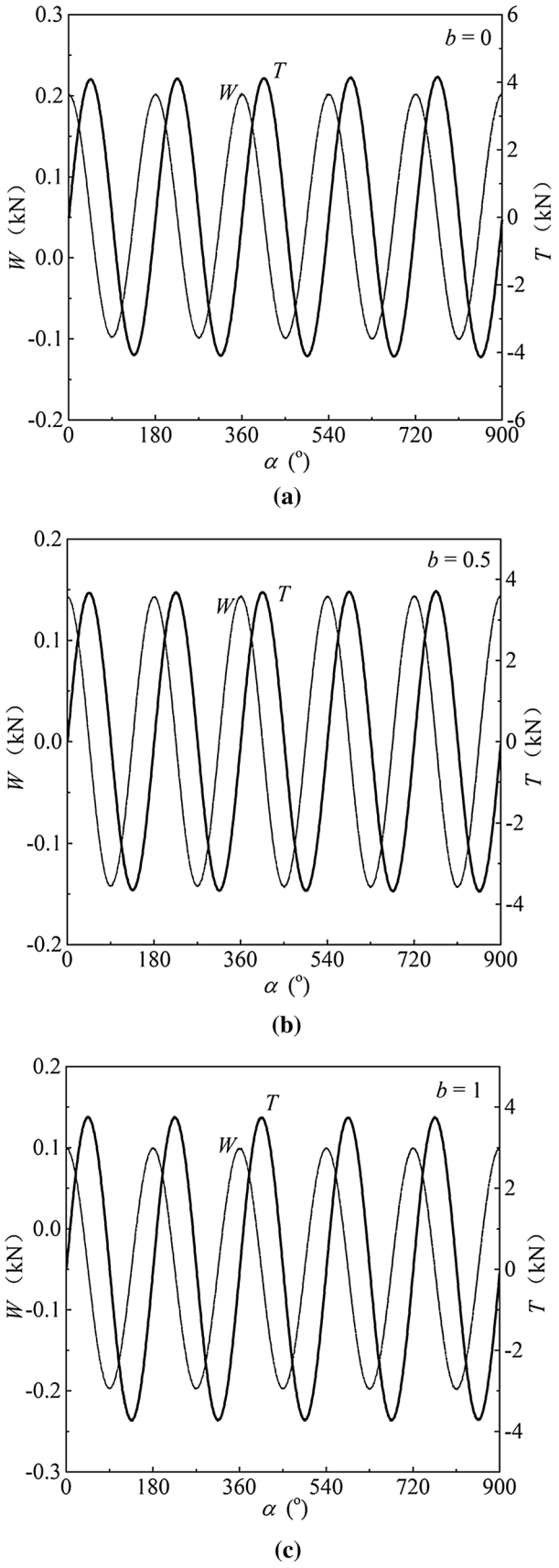

◀**Fig. 3** Variation of vertical load and torque under rotational shear: **a** $b = 0$; **b** $b = 0.5$; **c** $b = 1$

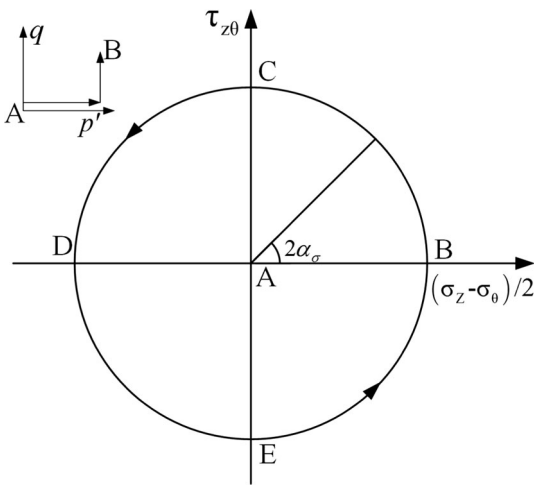

Fig. 4 Stress path under pure principal stress rotation

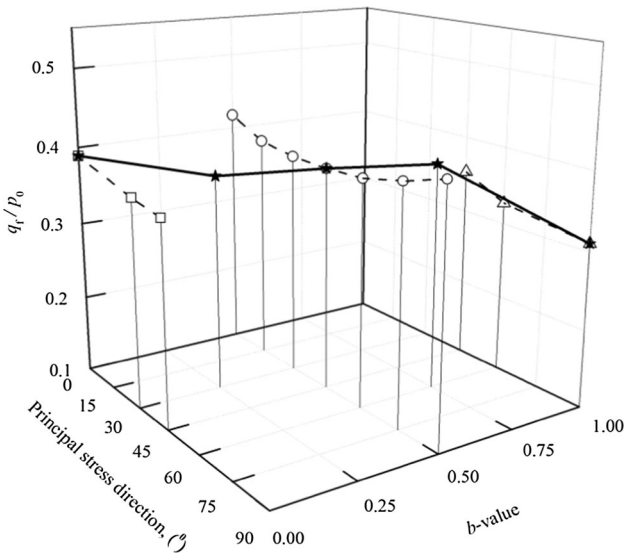

Fig. 5 Influence of b and α on shear strength of soft clay (Wang et al. [20])

axial direction under $b = 0$ and $b = 0.5$, and the value of compressive axial strain under $b = 0$ is obviously higher than that under $b = 0.5$. The specimen is subjected to tension in the axial direction under $b = 1$ during pure principal stress rotation, the value of tensile axial strain increases with increasing loading cycles. Same phenomenon was observed in undrained tests of intact soft clay conducted by Zhou et al. [31]. However, the impact of initial major principal stress direction ξ on the deformation behavior of natural soft clay is considerable and that will be discussed later.

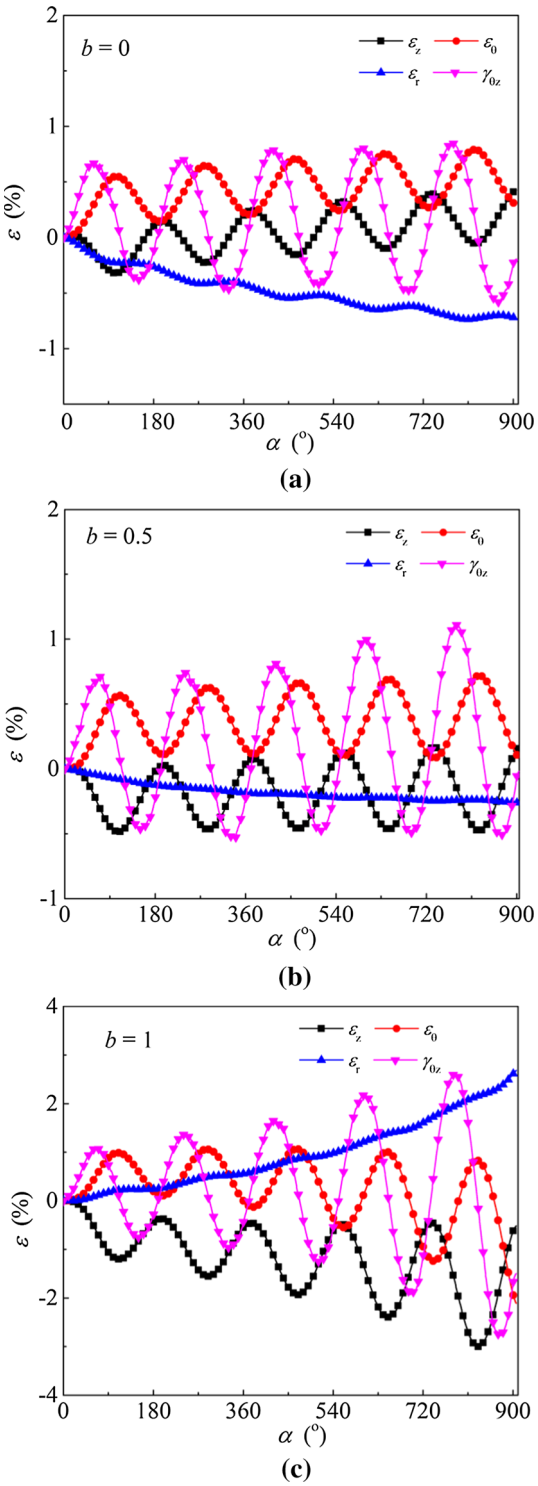

Fig. 6 Evolution of strain components for test series R1: **a** $b = 0$; **b** $b = 0.5$; **c** $b = 1$

The variations of ε_z under different coefficient b are similar for test series R2, R3, R4, R5, with varying ζ angles ($\zeta = 30°, 45°, 60°, 90°$) as shown in Fig. 7b–e. The evolutions of ε_z under $\zeta = 30°$ are shown in Fig. 7b, and the specimens are subjected to tension in axial direction under $b = 0.5$ and $b = 1$ during pure principal stress rotation. While for $b = 0$, axial strain kicks off in the tension side first and reaches its minimum value followed by an increase to the compressive side at the end of each cycle. In test series R5, the variations of axial strain plotted in Fig. 7e are contrary to that in R1, as shown in Fig. 7a. Axial strain ε_z increases in contractive side and reaches its maximum value, then decreases gradually. The specimen is subjected to compression in the axial direction for $b = 0$ and $b = 0.5$, and tension in axial direction for $b = 1$ under during pure principal stress rotation. It can be concluded that the effect of different b-values on the variation of axial strain is significant. The axial strain amplitude, that is, the difference between the maximum and minimum values of ε_z in one cycle, increases with increasing b-values.

The circumferential strains ε_θ are plotted against the major principal stress direction in Fig. 8 for test series R1, R2, R3, R4, R5, respectively. It can be seen clearly that the variations of ε_θ are contrary to the variations of ε_z. Circumferential strains ε_θ increases in compressive side in the initial stage and then decreases gradually, and circumferential strains ε_θ accumulate with the rotation of principal stress axis. With the same initial major principal stress direction ζ, the variations of ε_θ differ under different b-values. By comparing the generation trends of ε_θ in different test series, ε_θ is dominated by compression for $b = 0$ and tension for $b = 1$. The circumferential strain amplitude, that is, the difference between the maximum and minimum values of ε_θ in one cycle, increases with increasing b-values.

Figure 9a–e shows the evolution of torsional strain$\gamma_{z\theta}$ for different test series R1, R2, R3, R4, R5, respectively. For the initial major principal stress direction $\zeta = 0°$ and $\zeta = 90°$, the variations of torsional strains in each cycle are contrary. Take test series R1 shown in Fig. 9a as an example, in the first cycle (0°–180°), the torsional strain $\gamma_{z\theta}$ increases in contractive side and reaches its maximum value, then decreases gradually until reaches the minimum value. However, the torsional strain is symmetrical relative to the horizontal ordinate, and the torsional strain amplitude, difference between the maximum and minimum values of $\gamma_{z\theta}$ in one cycle, increases with increasing of b-values. However, the variations of torsional strains $\gamma_{z\theta}$ are dominated by tension in different tests under $\zeta = 30°, 45°, 60°$ during pure principal stress rotation, the torsional strain amplitude also increases with increasing b-values.

Other than the oscillation in variation of ε_z, $\gamma_{z\theta}$ and ε_θ, an approximately linear relationship between radial strain ε_r and major principal stress direction α is observed as shown in Fig. 10. It is similar to the results obtained by normally consolidated intact Hangzhou clay [31] and Shanghai clay [14], and it supports the fact that the variations of radial stresses are dependent of intermediate principal stress

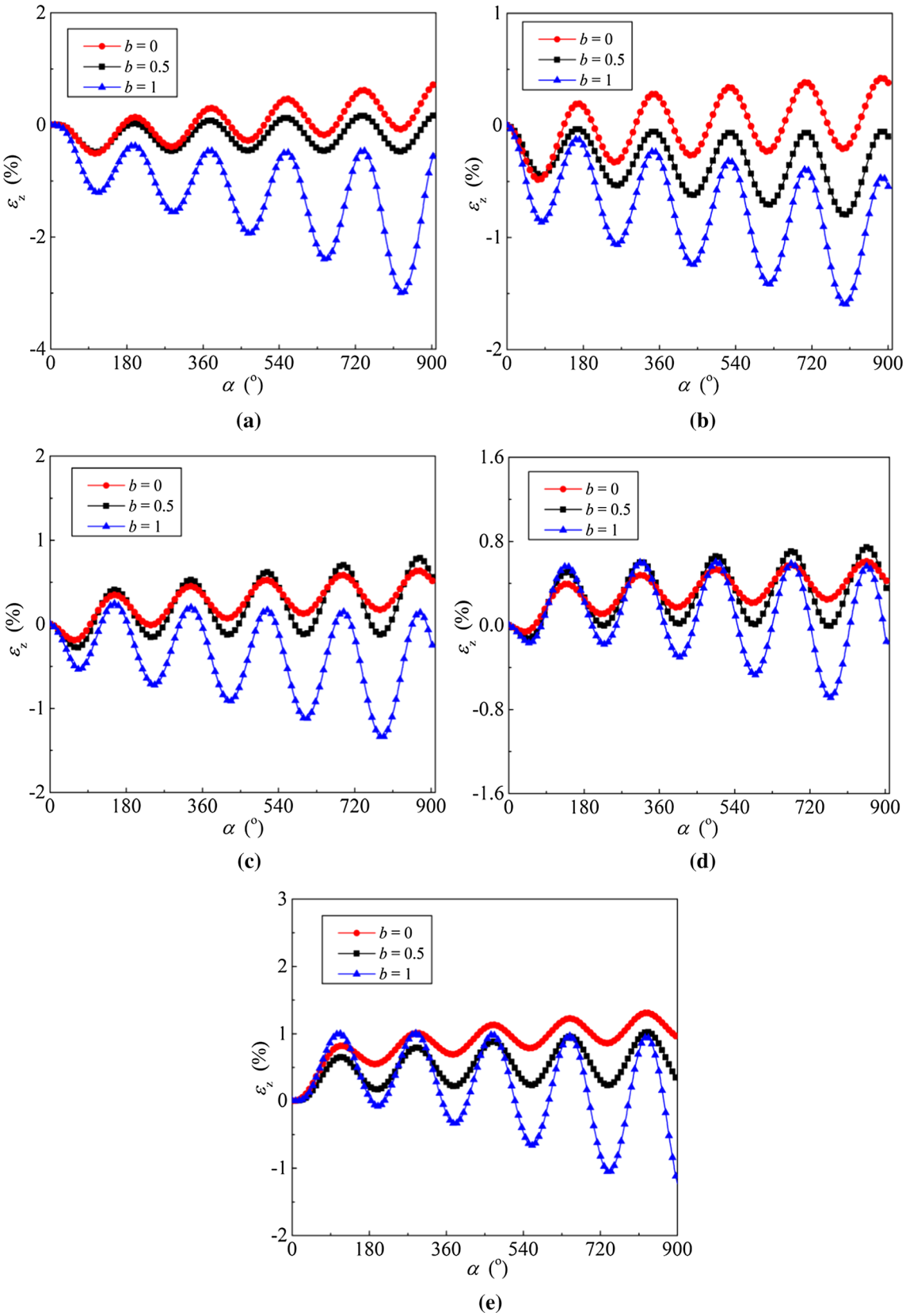

Fig. 7 Evolution of axial strain for different tests: **a** $\zeta = 0°$; **b** $\zeta = 30°$; **c** $\zeta = 45°$; **d** $\zeta = 60°$; **e** $\zeta = 90°$

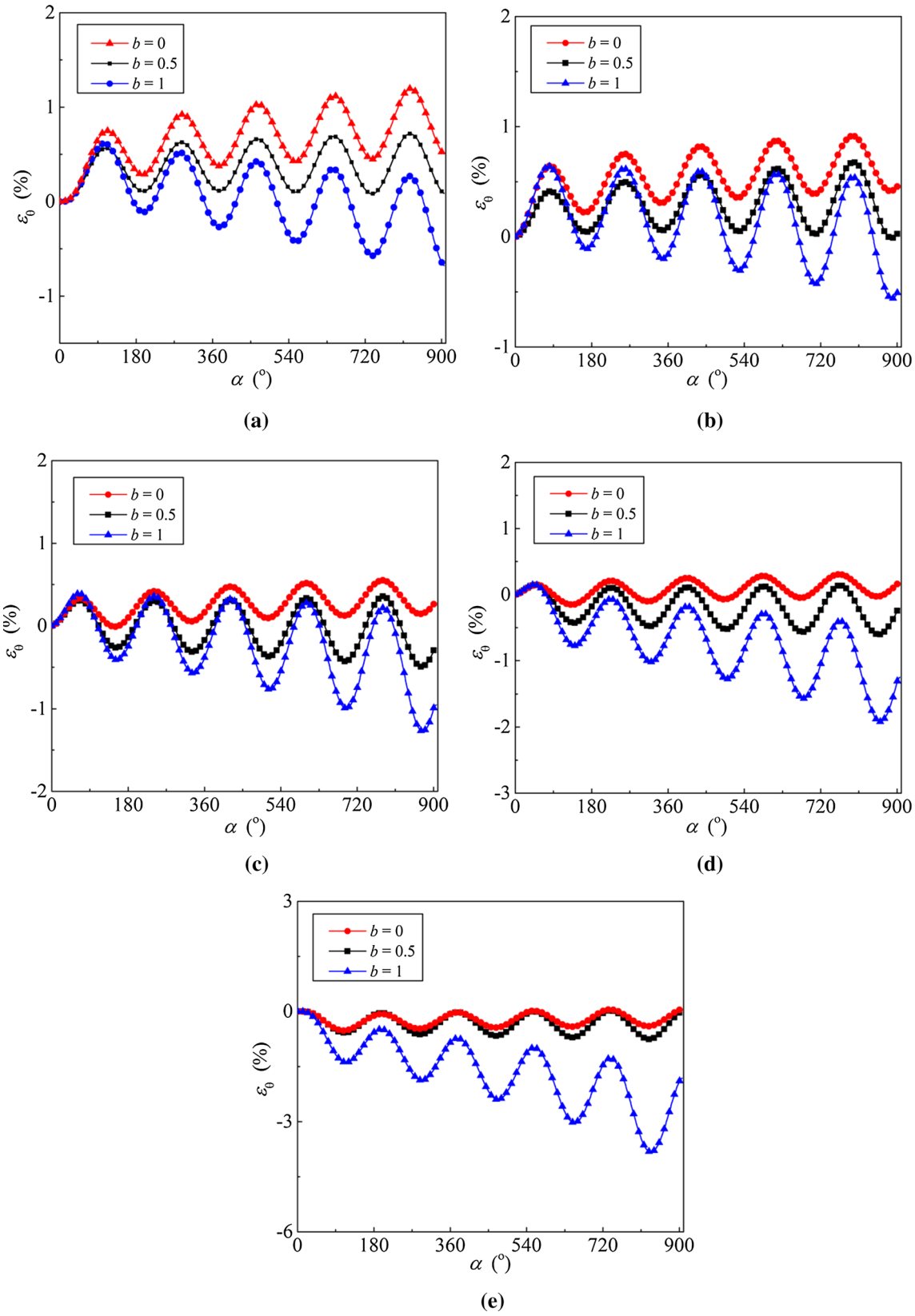

Fig. 8 Evolution of circumferential strain for different tests: **a** $\zeta = 0°$; **b** $\zeta = 30°$; **c** $\zeta = 45°$; **d** $\zeta = 60°$; **e** $\zeta = 90°$

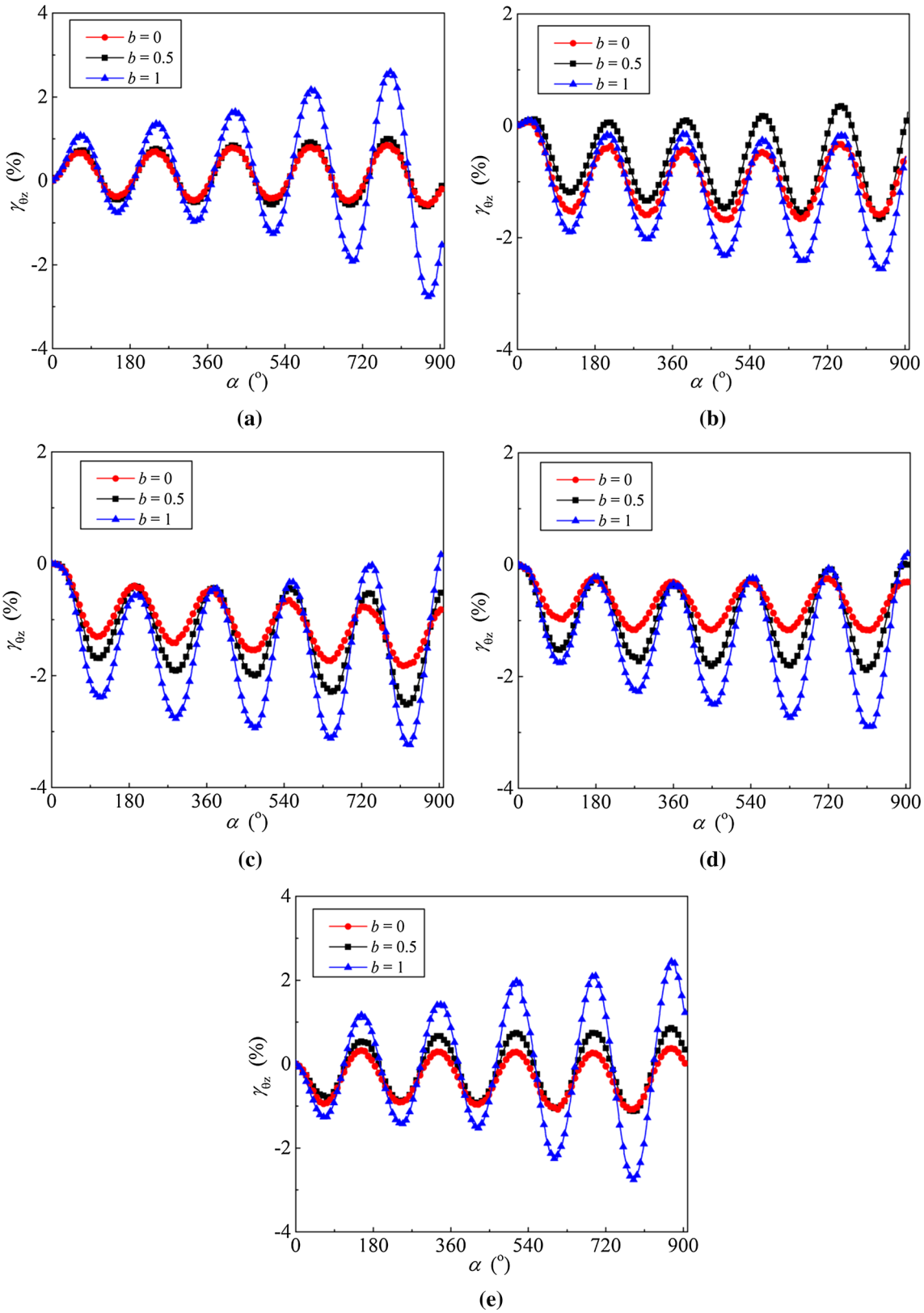

Fig. 9 Evolution of torsional strain for different tests: **a** $\zeta = 0°$; **b** $\zeta = 30°$; **c** $\zeta = 45°$; **d** $\zeta = 60°$; **e** $\zeta = 90°$

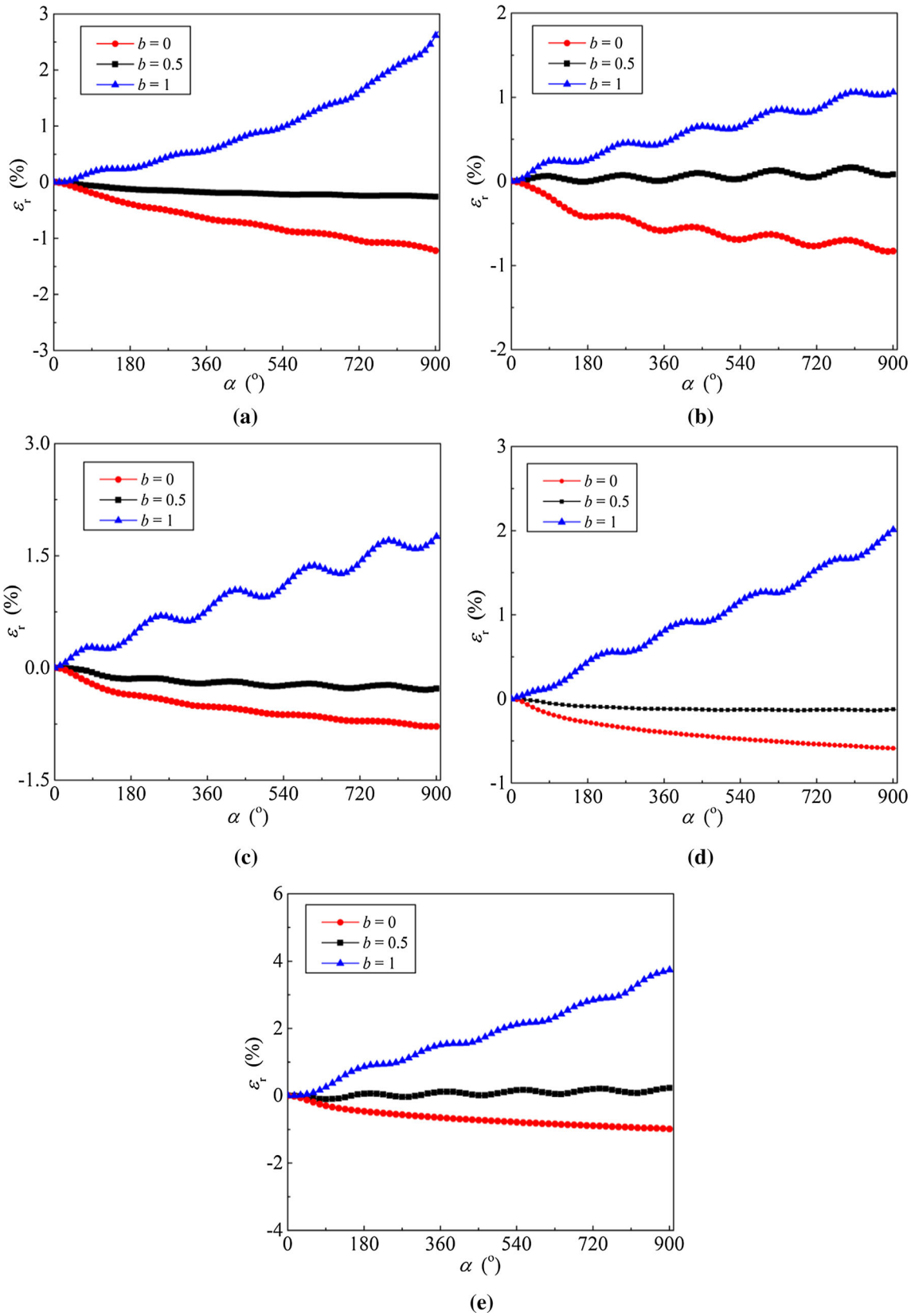

Fig. 10 Evolution of radial strain for different tests: **a** $\zeta = 0°$; **b** $\zeta = 30°$; **c** $\zeta = 45°$; **d** $\zeta = 60°$; **e** $\zeta = 90°$

coefficient. It needs to mention that when $b = 0.5$, very small radial strain developed during the whole rotation, and it indicates that the assumption of plane strain condition is reasonable when $b = 0.5$. And also, the radial strain ε_r accumulates in the tensile side for $b = 0$, and ε_r accumulates in the compressive side for $b = 1$. Wang et al. [20] investigated the influence of intermediate principal stress coefficient on the radial strain and gave the explanations as that, due to that the value of b reflects the constraint in the radial direction, the lower constraint under $b = 0$ leads to the occurrence of the extension radial strain ε_r. Higher contractive radial strain ε_r is finally induced due to easy compressive tendency in the radial direction, which is because the radial stress σ_r becomes the major principal stress under $b = 1$.

To compare influence of different stress histories on the strain components (ε_z, $\gamma_{z\theta}$, ε_θ, ε_r) under pure principal stress rotation, Figs. 11, 12, 13, 14 show the variation of strain components (ε_z, $\gamma_{z\theta}$, ε_θ, ε_r) with increasing α angles under different initial major principal stress directions ζ. It is obvious that the strain components are different under different initial major principal stress directions ζ.

Figure 11a–c presents the evolution of axial strain ε_z under $\xi = 0°$, 30°, 45°, 60°, 90° for $b = 0$, 0.5, 1, respectively. It can be obviously seen that with the same b-value, the variations of axial strain differ under different initial major principal stress directions ζ.

It can be seen in Fig. 11a, ε_z increases in tensile side in the first cycle under $b = 0$ for $\zeta = 0°$ and $\zeta = 30°$. At the end of cycle ($\alpha = 900°$), the specimen is subjected to contraction in the axial direction. With increasing initial major principal stress direction ζ, ε_z is dominated by contraction and increases in contractive side with the increase in loading cycles. For $b = 0$, $\zeta = 90°$, the axial strain

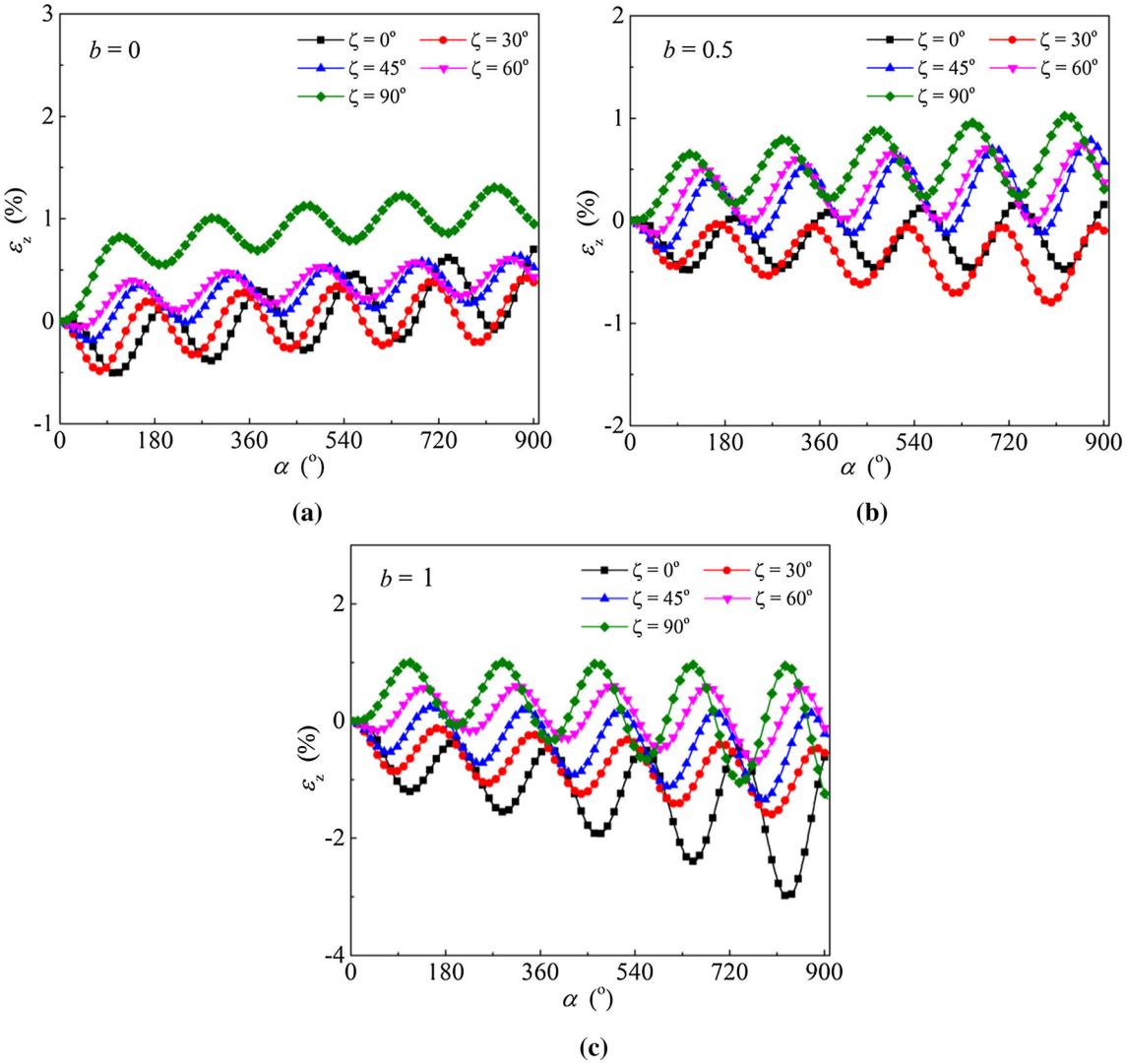

Fig. 11 Evolution of axial strain for different tests: **a** $b = 0$; **b** $b = 0.5$; **c** $b = 1$

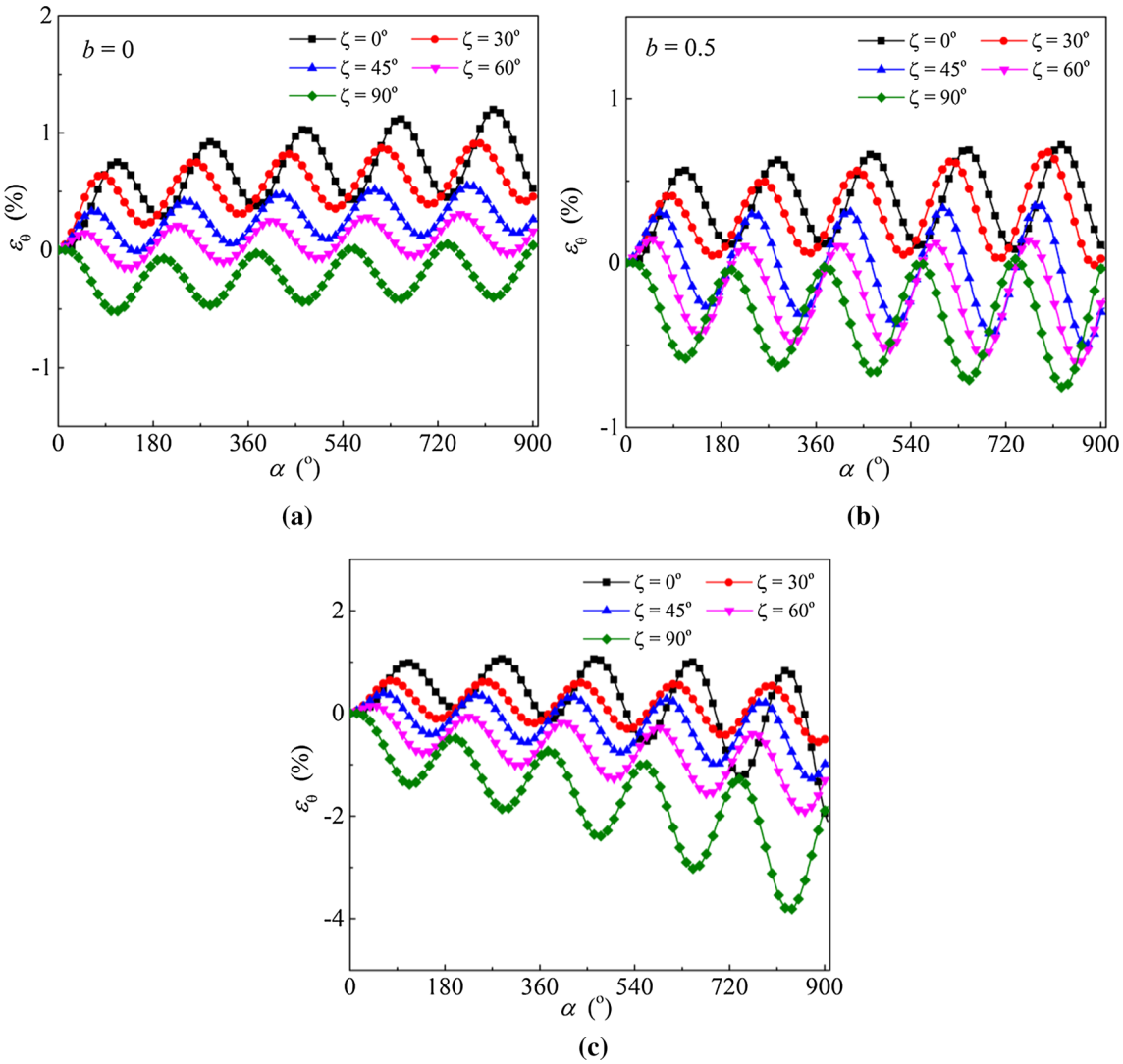

Fig. 12 Evolution of circumferential strain for different tests: **a** $b = 0$; **b** $b = 0.5$; **c** $b = 1$

increases rapidly during the first cycle ($\alpha = 0° \sim 180°$) and reaches 1.7% at the end of the first cycle ($\alpha = 180°$), and then the increasing rate of ε_z is slow with the rotation of principal stress axis. The variations of axial strain for different tests under $b = 0.5$ (Fig. 11b) and $b = 1$ (Fig. 11c) are similar to that under $b = 0$. However, when $b = 1$, the value of tensile axial strain for $\zeta = 0°, 30°, 45°$ is higher, and at the end of loading cycle ($\alpha = 900°$), the specimen is subjected to tension for all tests under $b = 1$, which is due to the impact of intermediate principal stress coefficient b.

The variations of circumferential strains ε_θ for different initial major principal stress directions under $b = 0, 0.5, 1$ are contrary to that of axial strains ε_z, as shown in Fig. 12. With the increase in initial major principal stress direction ζ, the circumferential strains increase and generate toward the tensile side. In each cycle, the amplitudes of circumferential strains are little difference for different initial principal stress directions ξ, and it can be concluded that circumferential strain amplitudes are merely influenced by ζ angles.

The evolutions of torsional strains $\gamma_{z\theta}$ for different initial major principal stress directions under $b = 0, 0.5, 1$ are shown in Fig. 13. It is obvious that the torsional strains $\gamma_{z\theta}$ are symmetrical relative to the horizontal ordinate for $\zeta = 0°$ and $\zeta = 90°$. The variations of torsional strains are similar for $\zeta = 30°$, $\zeta = 45°$ and $\zeta = 60°$; the torsional strain amplitudes are also approximately equal. It can be concluded that whether the specimens are subjected to contraction or tension are dependent on the initial major principal stress direction ζ.

As discussed before, the radial strains are approximately a linear relationship between radial strain ε_r and major principal stress direction α. However, the effect of different

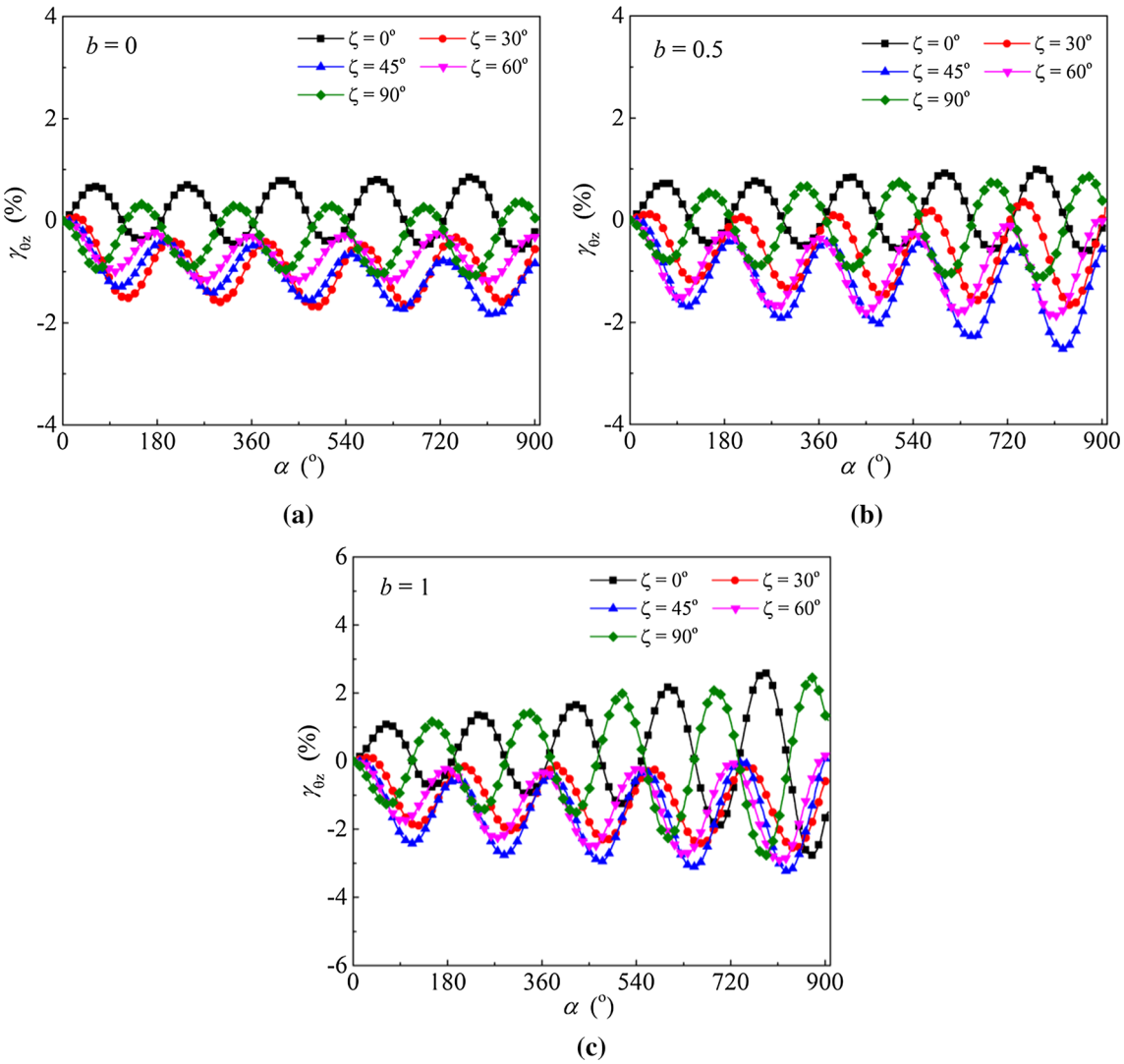

Fig. 13 Evolution of torsional strain for different tests: **a** $b = 0$; **b** $b = 0.5$; **c** $b = 1$

initial major principal stress directions ζ on the variation of radial strain is merely, as shown in Fig. 14. For $b = 0.5$, the radial strain is approximately equal to 0, the conclusion is consistent with that of natural soft clay under the fixed principal stress direction during shearing [24], and it indicates that the assumption of plane strain condition is reasonable when $b = 0.5$ [31].

The generations of pore water pressure under pure principal stress rotation for different series R1–R5 are shown in Fig. 15. Although the deviator stress and total mean stress are constant during pure principal stress rotation, pore water pressure accumulates significantly with the increase in principal stress direction, and clear fluctuations are observed. The pore water pressure generation is significant during the first cycle, and shows less volatility and grows approximately linearly. Moreover, the corresponding major principal stress directions are different when the peak value of pore water pressure occurs in different tests; it indicates that the generation of pore water pressure is significantly dependent on stress path. The observation is similar to the results obtained in undrained shear tests with fixed principal stress directions during shearing conducted by Kumruzzaman and Yin [6]. Comparing the generation of pore water pressure under different test series, it can be obtained that the rate of pore water pressure generation under $b = 0$ is much slower than that under $b = 0.5$ and 1. This observation is consistent with that observed in sand [28] and soft clay [31] under pure principal stress rotation.

Figure 16a–c presents the generation of pore water pressure under pure principal stress rotation for $b = 0$, 0.5, 1, respectively. Due to complex impact factors on accumulation of pore water pressure, the discreteness is larger under $b = 0$ and $b = 1$ than that under $b = 0.5$ with different initial major principal stress direction ζ applied.

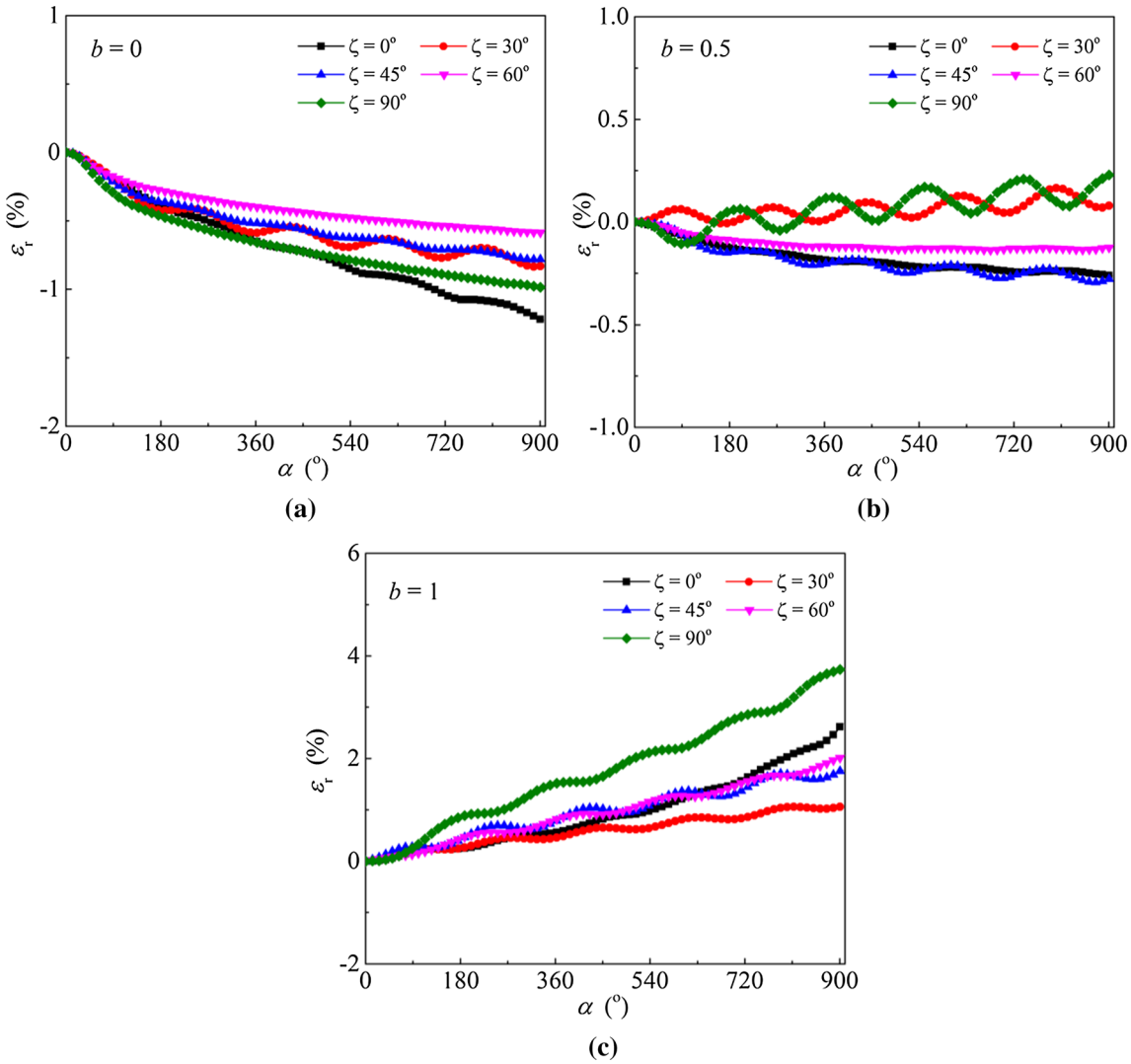

Fig. 14 Evolution of radial strain for different tests: **a** $b = 0$; **b** $b = 0.5$; **c** $b = 1$

When $b = 1$, larger values of pore water pressure occur when $\zeta = 0°$ and $\zeta = 90°$. It can be concluded that the changes in the direction of principal stress alone could lead to pore water pressure accumulation [28, 31]. Moreover, different values of pore water pressures generate under different initial major principal stress directions ζ. To the best knowledge, the accumulation further causes soil degradation; then, it should be considered in practice.

While the deviator stress is maintained constant during the tests, the clay specimens show hysteretic and plastic characteristics. The torsional shear stress–strain relationships of R1 under three cases of b-values are shown in Fig. 17, different cycles are plotted using different types of alignment. Where $N1$ represents the first cycle, and it is so on for $N2$–$N5$. It is obvious that the hysteretic loops of the torsional shear stress–strain curves occur during pure principal stress rotation. The hysteretic loops appear unclosed for the first cycle, it manifests the accumulation of plastic strain occur due to the rotation of principal stress direction alone. With the number of cycles increasing, significant stiffness degradation is observed and the hysteretic loops tend to be closed.

To have a better view of the impact of the coefficient b on the torsional shear stress–strain relationships, the first cycle ($N1$) and the third cycle ($N3$) are plotted under different b-values for different test series as shown in Figs. 18, 19, 20, 21, 22. It can be obviously seen that the stiffness degradation is more significant with increasing b-values. The observation agrees well with the tests on sand [19, 28] and clay [14, 31].

Dynamic modulus, as an important indicator measurement of soil stiffness under cyclic loading, has very important significance. Yang et al. [28] considered that the stiffness degradation is simply represented by the ratio between the secant modulus in the rth cycle of rotation shearing and the secant modulus in the first cycle of

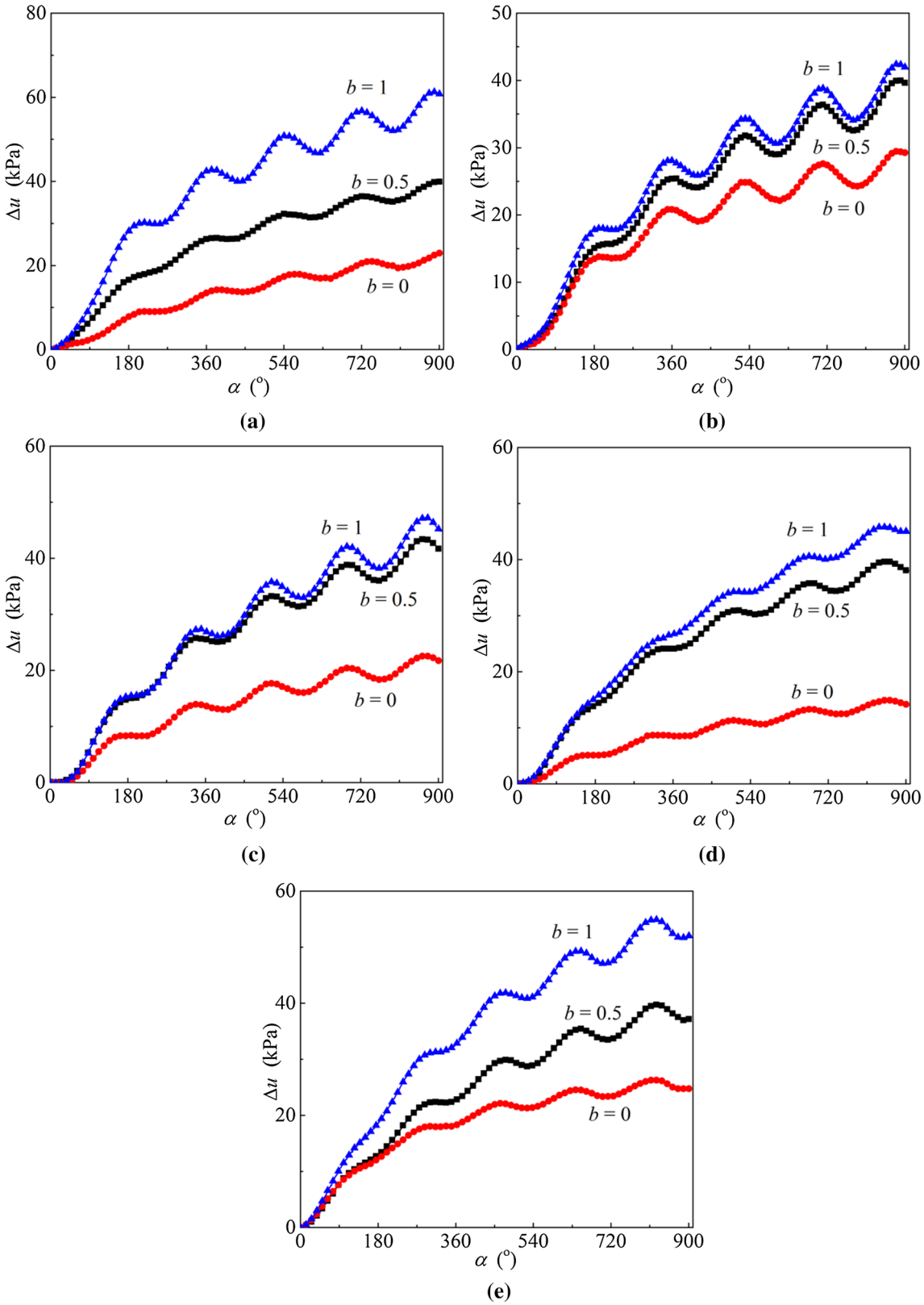

Fig. 15 Generation of pore water pressure under principal stress rotation for different tests: **a** $\zeta = 0°$; **b** $\zeta = 30°$; **c** $\zeta = 45°$; **d** $\zeta = 60°$; **e** $\zeta = 90°$

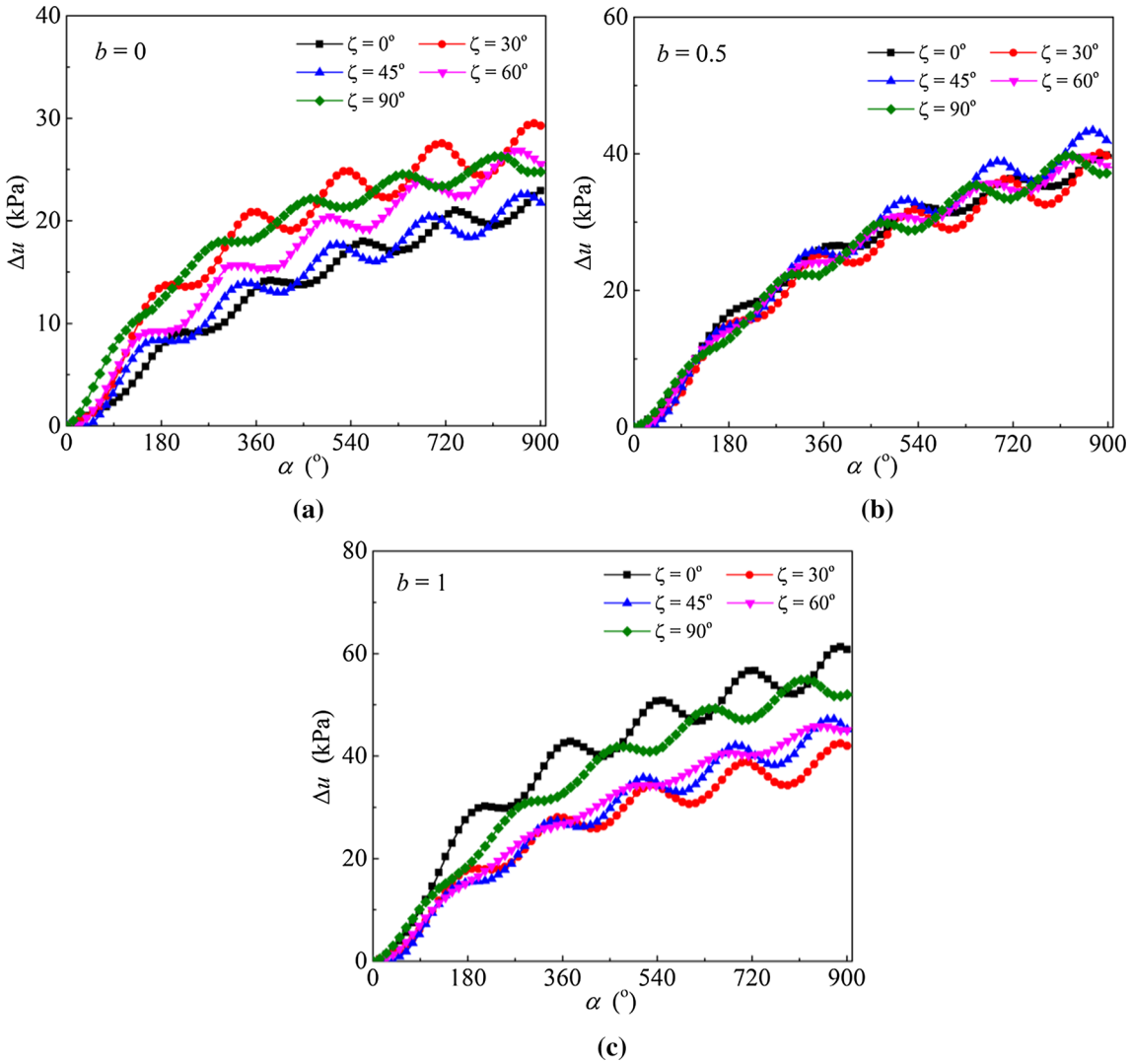

Fig. 16 Generation of pore water pressure under principal stress rotation for different tests: **a** $b = 0$; **b** $b = 0.5$; **c** $b = 1$

rotation, G_r/G_1. Soil with a high degradation index value will have a low degree of degradation [21].

The variations of stiffness ratio for different initial major directions and different b-values with the number of cycles are shown in Fig. 23. Figure 23a shows the variations of stiffness ratio for different b-values with $\zeta = 45°$, it is obvious that stiffness degradation occur under cyclic principal stress rotation. It can be also seen that the influence of b-values on the stiffness degradation is considerable. With increasing b-values, the stiffness ratio decreases. Influence of different initial major principal stress directions ζ under $b = 0.5$ on the stiffness ratio is presented in Fig. 23b. It can be seen that stiffness degradation is observed with pure principal stress rotation and different value of stiffness ratio is obtained with different ζ angles. It can be seen that the stiffness ratio with $\xi = 0°$ is larger than other tests in each cycle. With ζ changes from 30° to 90°, the corresponding stiffness ratio remains approximately unchanged in the first three cycles and then increase in the subsequent two cycles.

Many laboratory test results indicate that geo-materials always show non-coaxiality. Non-coaxiality is defined as the non-coincidence of the principal stress direction and the principal strain increment direction. Some researchers focused on the non-coaxial behavior of soil and found that it has very important influences on analysis and design in geotechnical engineering, the geotechnical design without considering the effects of non-coaxiality may be unsafe [1, 11, 14, 25, 27]. The collective results of deformation non-coaxiality provoked the development of conventional plastic theory to better predict inherent soil behaviors. As shown in Fig. 24, the strain paths of tests with $b = 0.5$ developed in the first rotation period are plotted, it is similar to the pattern presented by Miura et al. [8] and Qian et al. [14]. It can be obviously seen that the generation of the strain paths are dependent on the initial major principal

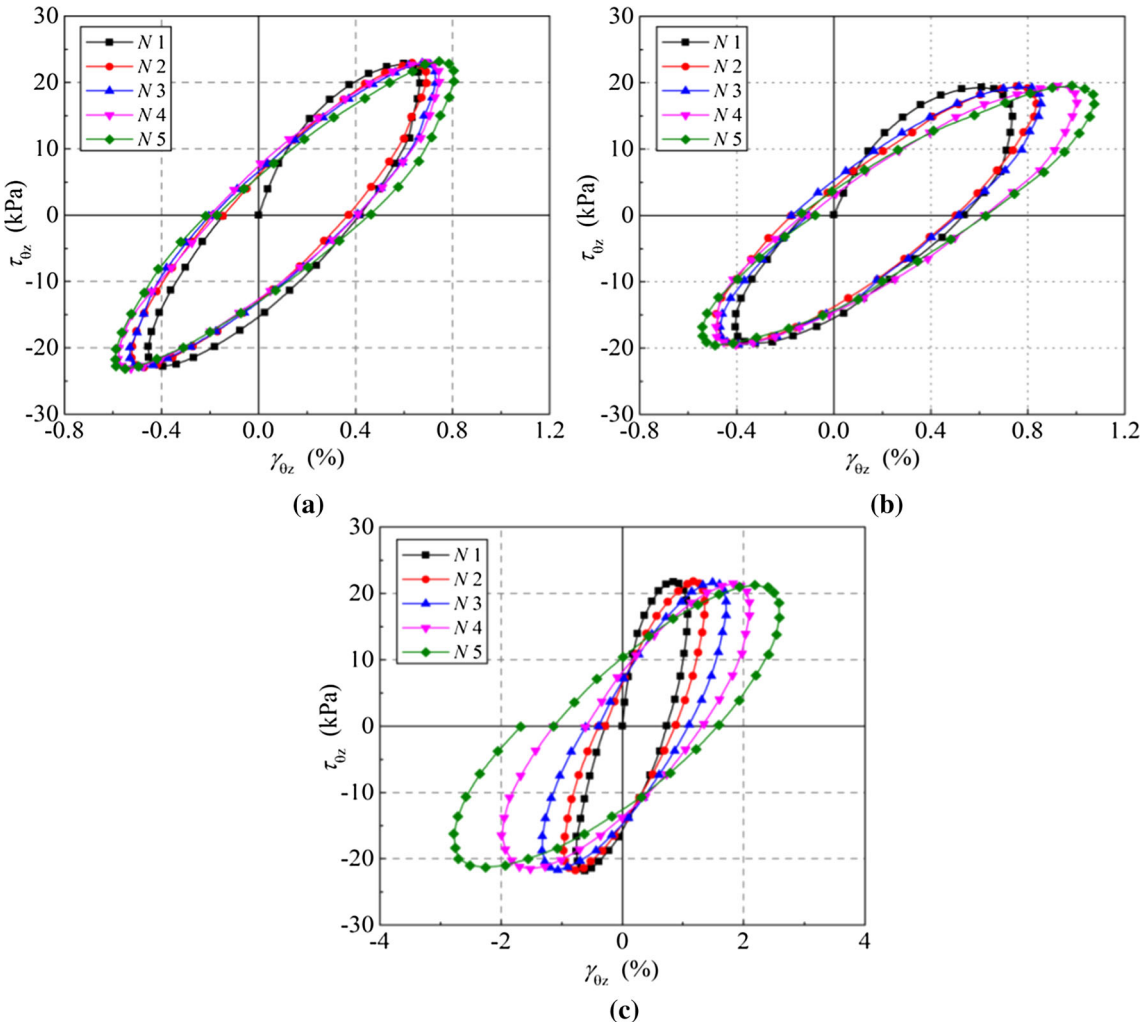

Fig. 17 Shear stress–strain relationship (R1): **a** $b = 0$; **b** $b = 0.5$; **c** $b = 1$

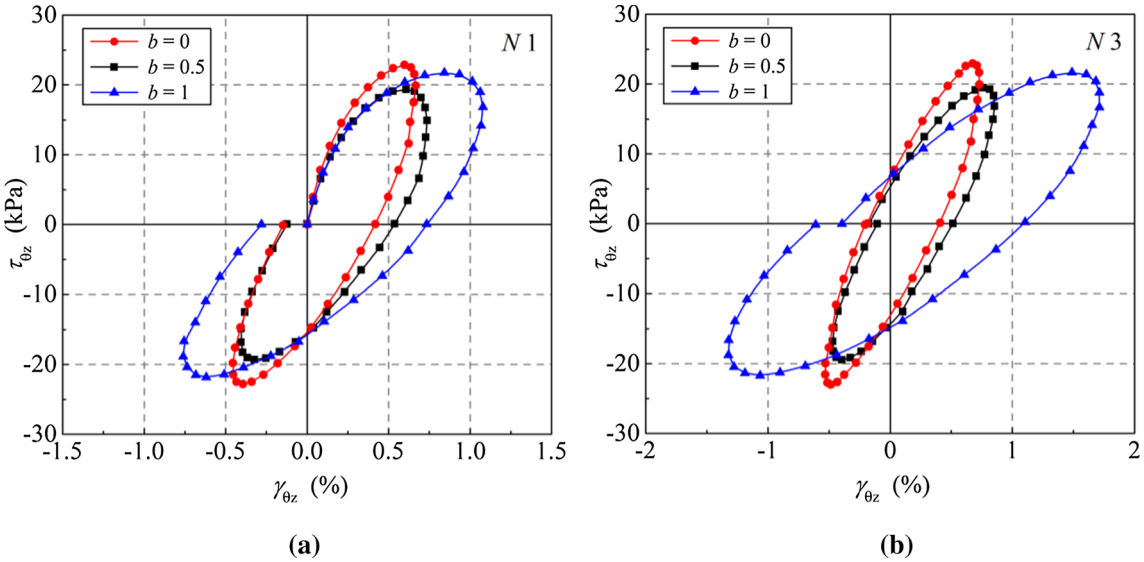

Fig. 18 Shear stress–strain relationships under different b-values (R1): **a** $N1$; **b** $N3$

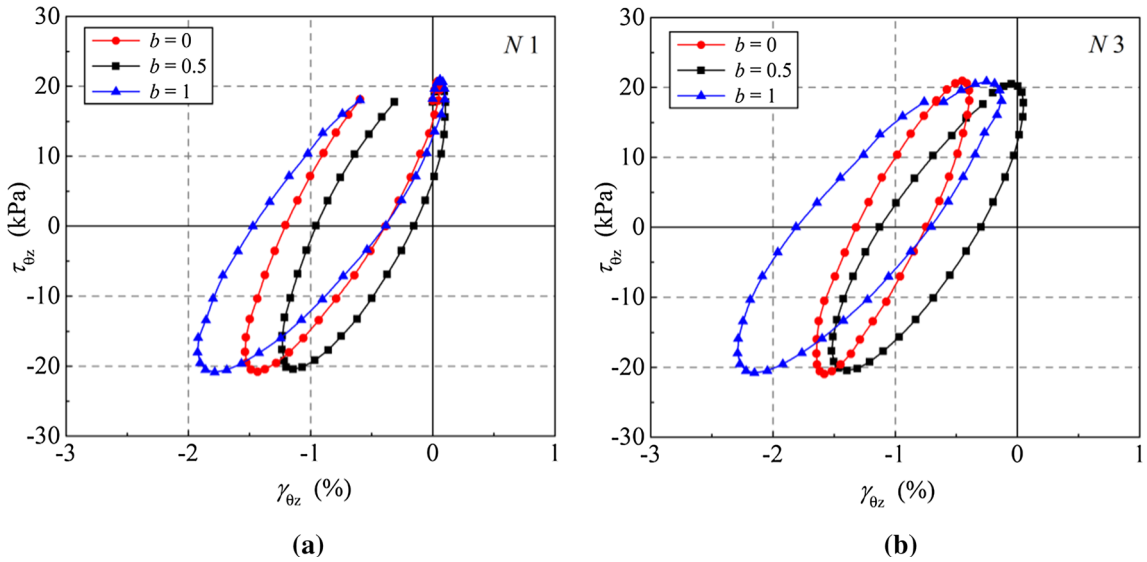

Fig. 19 Shear stress–strain relationships under different b-values (R2): **a** $N1$; **b** $N3$

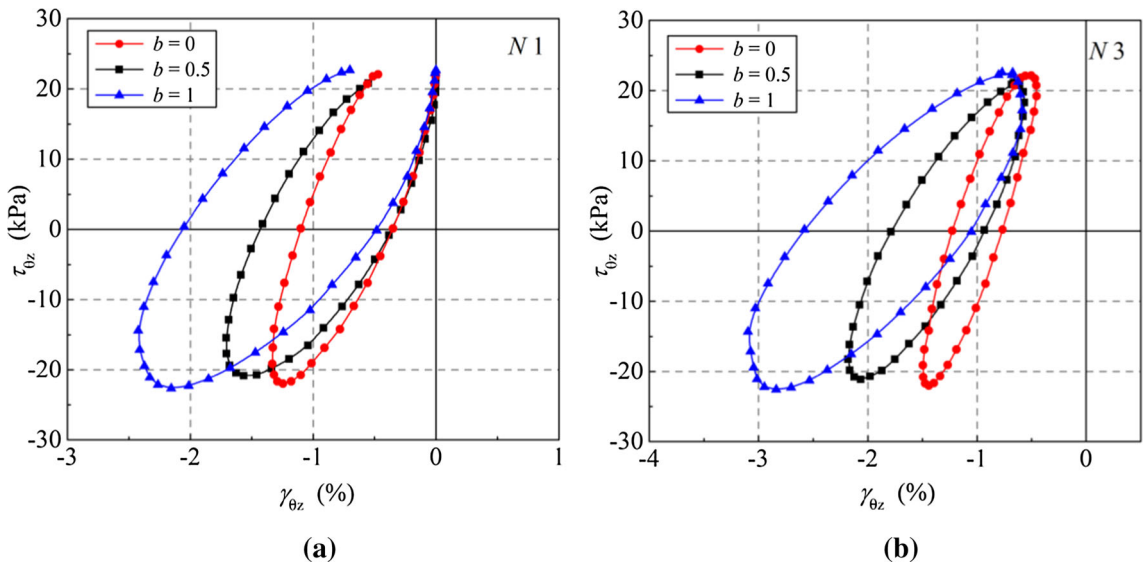

Fig. 20 Shear stress–strain relationships under different b-values (R3): **a** $N1$; **b** $N3$

stress direction. In addition, comparing with the stress paths shown in Fig. 4 during pure principal stress rotation, the strain paths are not consistent with the stress paths under the same test series, which can be concluded that non-coaxiality occur. It can also be obviously seen that the fashion of the strain paths are dependent on the initial major principal stress direction. It indicates that the anisotropic behavior resulting from the process of inclined consolidation may have considerable effects on the strain components and non-coaxial behavior of soft clay.

In this paper, due to that it is difficult to accurately separate the elastic strain increment from the total strain increment. According to the studies of Gutierrez et al. [1], the elastic strain increment can be disregarded as it takes much smaller proportion in the total strain increment than the plastic strain increment. The total strain increment is used in analysis of non-coaxiality, instead of the plastic strain increment. Then the degree of the non-coaxiality, β-degree, can be represented by the angle between the principal stress directions α and principal strain increment directions $\beta_{d\varepsilon}$, in which:

$$\beta = \beta_{d\varepsilon} - \alpha \tag{5}$$

$$\beta_{d\varepsilon} = \frac{1}{2}\tan^{-1}\frac{d\gamma_{z\theta}}{d\varepsilon_z - d\varepsilon_\theta} \tag{6}$$

To better study the effect of intermediate principal stress coefficient b on the variation of non-coaxiality during

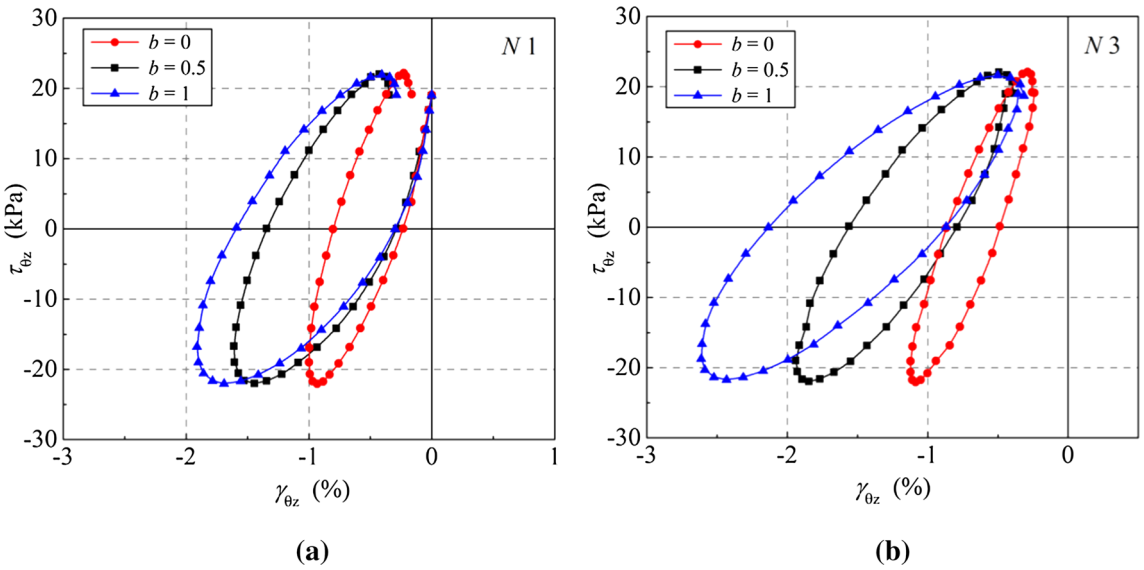

Fig. 21 Shear stress–strain relationships under different *b*-values (R4): **a** *N*1; **b** *N*3

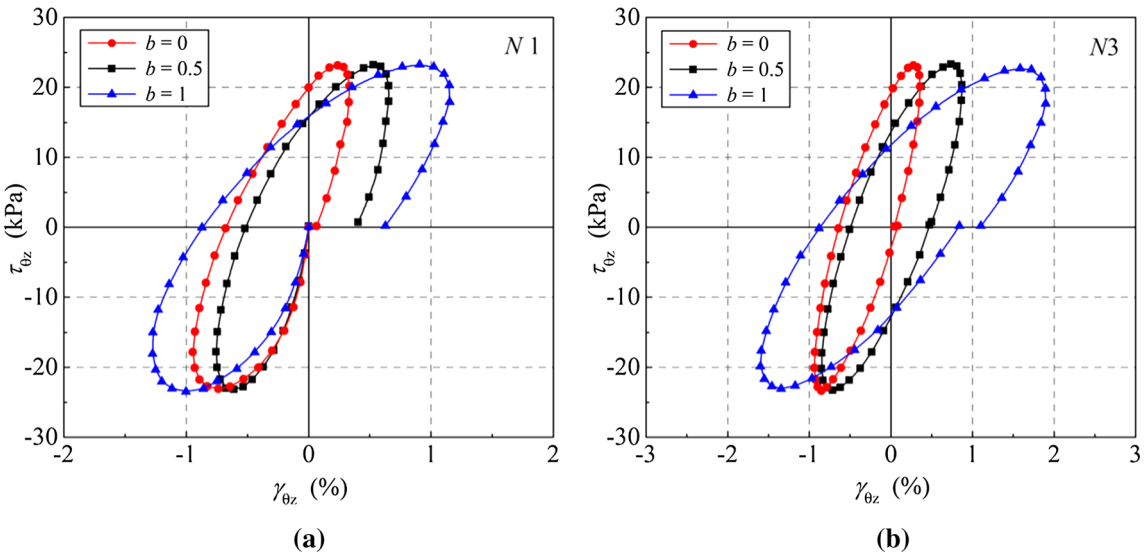

Fig. 22 Shear stress–strain relationships under different *b*-values (R5): **a** *N*1; **b** *N*3

rotation of principal stress axis, Fig. 25 illustrates the degrees of non-coaxiality angle against the major principal stress direction under $\zeta = 0°$ for the first and thirst cycle. Recalling Figs. 5 and 24, it can be obtained that non-coaxiality is closely related to strength anisotropy. With principal stress direction changes from 0° to 45° and 90° to 135°, the non-coaxiality is decreased corresponding to the strength variation of soft clay presented in Fig. 5. The results are consistent with the results obtained from normal consolidated Hangzhou soft clay [31] and Shanghai soft clay [14]. The variations of non-coaxiality against the major principal stress direction for the third rotation period shown in Fig. 25b are similar to that of the first rotation period. It can be also seen that the non-coaxiality decreases with increasing *b*-values. It suggests that the non-coaxiality increasing with cyclic stiffness stability at different *b*-values. As the value of *b* reflects the constraint in the redial direction, the lower constraint under $b = 0$ leads to the occurrence of extension radial strain. Then, the degrees of non-coaxiality are higher under $b = 0$ than the degrees of non-coaxiality under $b = 0.5$ and $b = 1$; it can be supported with the generation of non-coaxiality results reported in the literature [19, 24].

To investigate the effect of initial major principal stress direction ζ on the variation of non-coaxiality, Fig. 26 shows the relationship between the degrees of non-coaxiality at the first rotation period *N*1 (0°–180°) and the third rotation period *N*3 (360°–540°). Different initial major

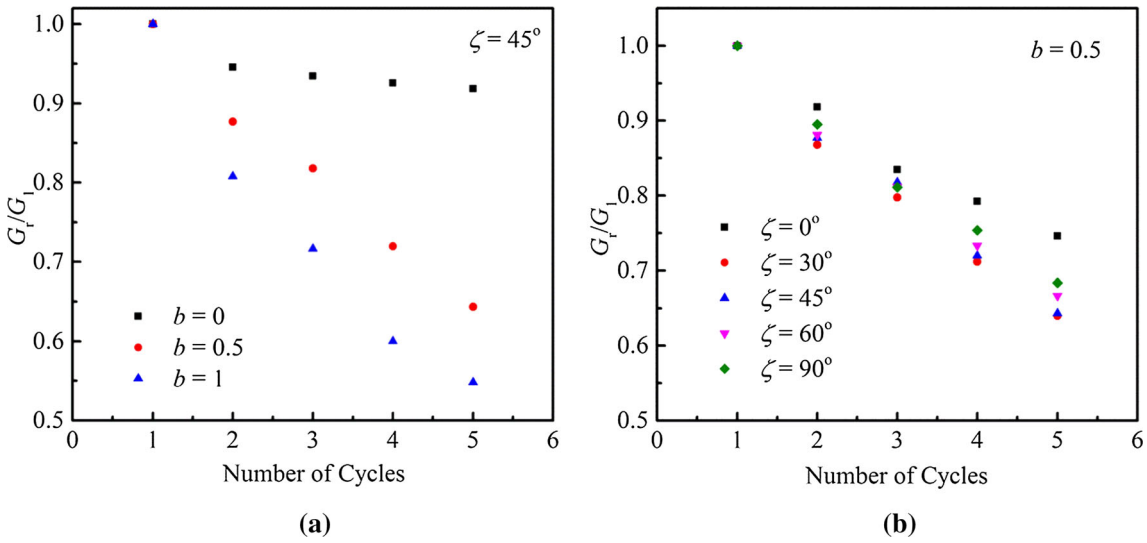

Fig. 23 Variation of stiffness ratio for **a** different b-values with $\zeta = 45°$; **b** different ζ angles with $b = 0.5$

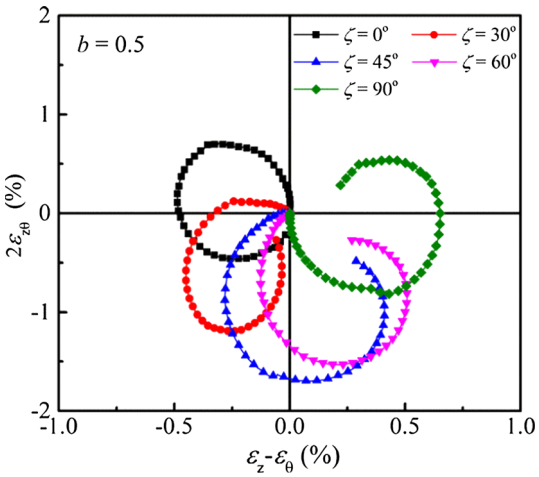

Fig. 24 Strain paths of test with $b = 0.5$ under pure principal stress rotation

principal stress direction ζ ($\zeta = 0°$, 30°, 45°, 60°, 90°) under $b = 0.5$ are plotted against major principal stress direction. Even some similar evolutions occur, some different evolutions exists for different initial major principal stress directions ζ. The similar situation is that the initial degree of non-coaxiality approximately equals to 45° at the initial loading. Then, it can be obtained that same variation of non-coaxiality occurs when $\zeta = 0°$ and $\zeta = 90°$, contracts to that of $\zeta = 45°$. And also, the same variation of non-coaxiality occurs when $\zeta = 30°$ and $\zeta = 60°$. The corresponding major principal stress direction to the peak value of ζ-angles is different. For example, a difference of $\alpha = 15°$ exists when the peak value of ζ-angle occurs between $\zeta = 0°$ and $\zeta = 90°$. It can concluded that the non-coaxiality of soft clay is influenced by initial major principal stress direction. However, the maximum and minimum value of non-coaxiality in each period is approximate the same, and it means that the influence of ζ-angle on the maximum and minimum value of non-coaxiality in each period is slight.

4 Conclusions

This paper investigates the undrained behavior of soft clay with different initial major principal stress directions under pure principal stress rotation. The influence of the intermediate principal stress coefficient b is investigated and discussed. The major experimental observations and conclusions can be summarized as follows:

(1) During pure principal stress rotation, the variation of the strain components depends on both the initial major principal stress direction ξ and the intermediate principal stress coefficient b. The radial strain is mainly influenced by b-values, and when $b = 0.5$, the radial strain is approximately equal to 0, it indicates that the assumption of plane strain condition is reasonable when $b = 0.5$

(2) Although the principal stress axes rotate alone, the pore water pressure accumulates. The pore water pressure generation is significant during the first cycle, and shows less volatility and grows approximately linearly. The generation of pore water pressure is significantly dependent on stress path. The rate of pore water pressure generation under $b = 0$ is much slower than that under $b = 0.5$, and the discreteness is larger under $b = 0$ and $b = 1$ than that under $b = 0.5$ with different initial major principal stress directions.

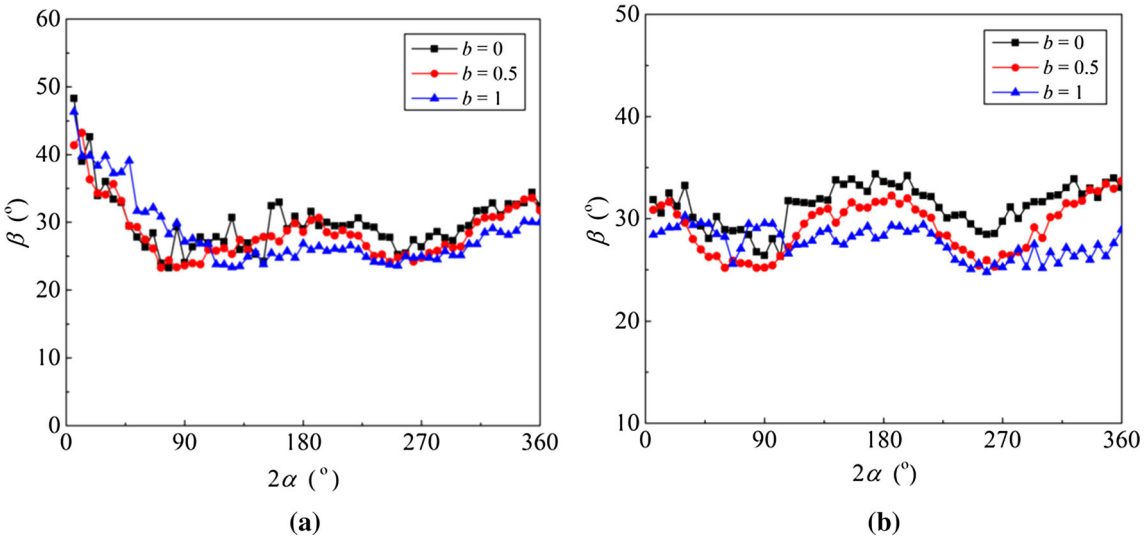

Fig. 25 The relationship between degrees of non-coaxiality and principal stress direction with $\zeta = 0°$ for **a** first cyclic period ($N1$); **b** third cyclic period ($N3$)

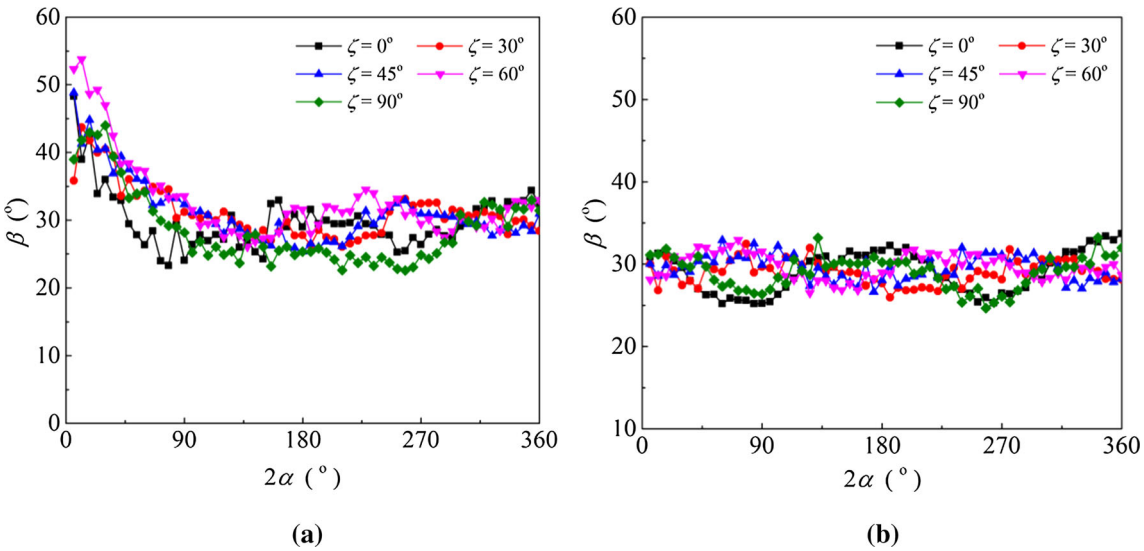

Fig. 26 The relationship between degrees of non-coaxiality and principal stress direction with $b = 0.5$ for **a** first cyclic period ($N1$); **b** third cyclic period ($N3$)

(3) The hysteretic loops of the shear stress–strain curves occur under different b-values and different initial major principal stress directions. The hysteretic loops appear unclosed for the first cycle, and it manifests the accumulation of plastic strain occur. The stiffness degradation is more significant with increasing b-values. The influence of initial major principal stress directions on the shear stress–strain relationships is significant.

(4) Stiffness degradation occurs under pure principal stress rotation. The influence of b-values and ζ angles on the stiffness degradation is considerable. With increasing b-values, the stiffness ratio is decreasing. The stiffness ratio with $\xi = 0°$ is larger than other tests in each cycle; with ζ angle changes from 30° to 90°, the corresponding stiffness ratio remains unchanged in the first three cycles and increase in subsequent two cycles.

(5) Anisotropic behavior resulting from the process of inclined consolidation have considerable effects on the strain components and non-coaxial behavior of soft clay. The b-values had a significant influence on non-coaxiality of soft clay, the degrees of non-coaxiality decrease with increasing b-values. The variation trend of non-coaxiality of soft clay is influenced by initial major principal stress direction,

but the influence of ζ-angle on the maximum and minimum value of non-coaxiality in each period is slight.

Acknowledgements This work present in this paper was supported by the National Key Research and Development Program of China (Grant No. 2016YC0800205); National Natural Science Foundation of China (Grant No. 51639002); "111" Project under No. B13024; Key Laboratory of Ministry of Education for Geomechanics and Embankment Engineering, Hohai University; China Postdoctoral Science Foundation (2017M610461). This financial support is gratefully acknowledged.

References

1. Gutierrez M, Ishihara K, Towhata I (1991) Flow theory for sand during rotation of principal stress direction. Soils Found 31:121–132
2. Hight DW, Gens A, Symes MJ (1983) The development of a new hollow cylinder apparatus for investigating the effects of principal stress rotation in soils. Géotechnique 33(4):355–383
3. Ishihara K, Towhata I (1983) Sand response to cyclic rotation of principal stress directions as induced by wave loads. Soils Found 23(4):11–26
4. Jardine RJ, Smith PR (1991) Evaluating design parameters for multi-stage construction. In: Proceedings of international conference on geotechnical engineering for coastal development, Yokosuka, pp 197–202
5. Kirkgard MM, Lade PV (1993) Anisotropic three-dimensional behavior of a normally consolidated clay. Can Geotech J 30(5):848–858
6. Kumruzzaman M, Yin JH (2010) Influences of principal stress direction and intermediate principal stress on the stress–strain–strength behaviour of completely decomposed granite. Can Geotech J 47(2):164–179
7. Lade PV, Kirkgard MM (2000) Effects of stress rotation and changes of *b*-values on cross-anisotropic behavior of natural, K0-consolidated soft clay. Soils Found 40(6):93–105
8. Miura K, Miura S, Toki S (1986) Deformation behavior of anisotropic dense sand under principal stress rotation. Soils Found 26(1):36–52
9. Nakata Y, Hyodo M, Murata H, Yasufuku N (1998) Flow deformation of sands subjected to principal stress rotation. Soils Found 38(2):115–128
10. Nishimura S, Minh N, Jardine R (2007) Shear strength anisotropy of natural London clay. Geotechnique 57(1):49–62
11. Qian J, Yang J, Huang M (2008) Three-dimensional non-coaxial plasticity modelling of shear band formation in geomaterials. J Geotech Eng ASCE 134(4):322–329
12. Qian J-g, You Z, Huang M, Gu X (2013) A micromechanics-based model for estimating localized failure with effects of fabric anisotropy. Comput Geotech 50:90–100
13. Qian J, Wang Y-G, Yin Z-Y, Huang M-S (2016) Experimental identification of plastic shakedown behavior of saturated clay subjected to traffic loading with principal stress rotation. Eng Geol 214:29–42
14. Qian JG, Du ZB, Yin ZY (2017) Cyclic degradation and non-coaxiality of soft clay subjected to pure rotation of principal stress directions. Acta Geotech 2018(13):943–959
15. Shen Y, Zhou J, Gong XN, Liu HL (2008) Intact soft clay's critical response to dynamic stress paths on different combinations of principal stress orientation. J Cent South Univ Technol 15:147–154
16. Shibuya S, Hight DW, Symes MJ (1984) Discussion on the paper by Ishihara and Towhata (1983). Soils Found 24(3):107–110
17. Symes MJ, Gens A, Hight DW (1984) Undrained anisotropy and principal stress rotation in saturated sand. Géotechnique 34(1):11–27
18. Symes MJ, Gens A, Hight DW (1988) Drained principal stress rotation in saturated sand. Géotechnique 38(1):59–81
19. Tong ZX, Zhang JM, Yu YL, Zhang G (2010) Drained deformation behavior of anisotropic sands during cyclic rotation of principal stress axes. J Geotech Geoenviron Eng 136(11):1509–1518
20. Wang YK, Guo L, Gao YF, Qiu Y, Hu XQ, Zhang Y (2016) Anisotropic drained deformation behavior and shear strength of natural soft marine clay. Mar Georesour Geotechnol 34(5):493–502
21. Wang Y, Gao Y, Guo L, Cai Y, Li B, Qiu Y, Mahfouz AH (2017) Cyclic response of natural soft marine clay under principal stress rotation as induced by wave loads. Ocean Eng 129:191–202
22. Wang Y, Gao Y, Li B, Fang H, Wang F, Guo L, Zhang F (2017) One-way cyclic deformation behavior of natural soft clay under continuous principal stress rotation. Soils Found 57(6):1002–1013
23. Wang Z, Yang Y, Yu H-S (2017) Effects of principal stress rotation on the wave–seabed interactions. Acta Geotech 12:97–106
24. Wang Y, Gao Y, Guo L, Yang Z (2018) Influence of intermediate principal stress and principal stress direction on drained behavior of natural soft clay. Int J Geomech 18(1):04017128
25. Wang Y, Gao Y, Cai Y, Guo L (2018) Effect of initial state and intermediate principal stress on non-coaxiality of soft clay involved cyclic principal stress rotation. ASCE Int J Geomech 18(7):04018081
26. Xiong H, Guo L, Cai Y, Yang Z (2016) Experimental study of drained anisotropy of granular soils involving rotation of principal stress direction. Eur J Environ Civ Eng 20(4):431–454
27. Yang Y, Yu HS (2006) A non-coaxial critical state soil model and its application to simple shear simulations. Int J Numer Anal Meth Geomech 30(13):1369–1390
28. Yang ZX, Li XS, Yang J (2007) Undrained anisotropy and rotational shear in granular soil. Géotechnique 57(4):371–384
29. Zdravković L, Jardine RJ (2001) The effect on anisotropy of rotating the principal stress axes during consolidation. Géotechnique 51(1):69–83
30. Zhou J, Xu CJ (2014) Impact of shear stress on strain and pore water pressure behavior of intact soft clay under principal stress rotation. Geotech Test J 37(3):1–16. https://doi.org/10.1520/GTJ20120189
31. Zhou J, Yan J, Xu C, Gong X (2013) Influence of intermediate principal stress on undrained behavior of intact clay under pure principal stress rotation. Math Probl Eng 950143:1–10